Highlights:

- An obstacle-related drift is created along an uplifted ridge and mud volcano
- drift-architecture and bottom current strength differ from the Cadiz-CDS
- Mud extrusions interfere with bottom currents and sedimentation patterns
- CWC mounds are present, incorporated within the sedimentary sequence

*Manuscript
Click here to download Manuscript: draft paper_final version.docx Click here to view linked References

Stratigraphy and palaeoceanography of a topography-controlled contourite drift in the Pen Duick area, southern Gulf of Cadiz

Vandorpe T.[1], Van Rooij, D.[1], de Haas, H.[2]

[1] Ghent University, Department of Geology & Soil Science, Renard Centre of Marine Geology, Krijgslaan 281 S8, 9000 Ghent, Belgium

[2] NIOZ Royal Netherlands Institute for Sea Research, Department of Marine Geology, P.O. Box 59, 1790 AB Den Burg, The Netherlands

Corresponding author:

Vandorpe Thomas

Krijgslaan 281, S8

9000 Gent

Belgium

Email: Thomas.vandorpe@ugent.be

Abstract

The northern part of the Gulf of Cadiz has and still is receiving a lot of attention from the scientific community due to (amongst others) the recent IODP Expedition 339. On the contrary, the southern part of the Gulf received far less attention, although mud volcanoes, diapiric ridges and cold-water corals are present in this region. The El Arraiche mud volcano field is characterized by a compressive regime (opposed to the extensive regime in most of the Gulf), creating several ridges and aiding the migration of hydrocarbons towards the surface. This study presents seismic and multibeam evidence for the existence of a contourite drift along the southwestern flanks of the Pen Duick escarpment (PDE) and Gemini mud volcano, within the El Arraiche mud volcano field. From the start of the Quaternary, when the escarpment started to lift and the mud volcano originated, contouritic deposition was initiated at the foot of both topographies. Initially, fairly low-speed bottom currents gave rise to sheeted drift deposits, affected by the uplift of the PDE or extrusion of mud. From the Mid-Pleistocene onwards, separated mounded drift deposits formed due to intensified bottom currents. An AAIW origin for the drift is proposed based on CTD data, whereas the influence of the Mediterranean Outflow Water (MOW) is not observed. Moreover, the changes recorded within this contourite drift differ from the MOW-dominated contourite depositional system in the northern Gulf of Cadiz, as drift deposits only occur as early as the base of the Quaternary (compared to the Early-Pliocene for the north) and mounded drift deposits only occur from the Middle-Pleistocene onwards (compared to the Early-Pleistocene). Cold-water coral mounds have been found within and on top of the sedimentary sequence at the foot of the PDE. This implies that environmental conditions in which cold-water corals thrive were present in the past at the foot of the PDE and not only on top.

Keywords: Gulf of Cadiz, Contourite drift, Pen Duick escarpment, mud volcano, seismic stratigraphy, Antarctic Intermediate Water

Highlights:

- An obstacle-related drift is created along an uplifted ridge and mud volcano

- drift-architecture and bottom current strength differ from the Cadiz-CDS
- Mud extrusions interfere with bottom currents and sedimentation patterns
- CWC mounds are present, incorporated within the sedimentary sequence

1. Introduction

Contourite deposits have first been recognized in the 1960's (Heezen et al., 1966) and were initially exclusively associated to thermohaline currents. Especially the deposits along the eastern North American margin, shaped by the western boundary undercurrent, have been studied (Locker and Laine, 1992; Mccave and Tucholke, 1986; Schneider et al., 1967). From then onwards, gradually a larger variety of contourite expressions, both in small or large scale, have been discovered (Duarte and Viana, 2007; Faugères and Stow, 1993a; Faugères and Stow, 1993b; Hernández-Molina et al., 2011). Other factors, as obstacles and internal waves, are now also acknowledged for being able to create contourite deposits (Hernández-Molina et al., 2006a; Preu et al., 2013; Rebesco et al., submitted). As a consequence, the definition of contourites has been adapted to sediments deposited or significantly affected by bottom currents (Rebesco et al., 2005; Stow et al., 2002). Not only depositional, but erosional features (furrows, moats, scours, …) are generated as well by bottom currents (Hernández-Molina et al., 2006b). Due to their enhanced sedimentation rates, contourites are ideal recorders for palaeoclimatological and palaeoceanographic information, since they are influenced by bottom currents and their association with climate is well established (Cacho et al., 2000; Frigola et al., 2008; Llave et al., 2007). Due to the important role of bottom current in sorting grain size classes, the economic potential of these deposits as reservoir systems may not be underestimated (Antich et al., 2005; Llave et al., 2005; Rebesco et al., submitted; Viana et al., 2007). Besides their ability to deposit laterally continuous muddy contourite sheets, operating as an impermeable seal, long-lasting bottom currents may also create extensive and "clean" sand sheets; e.g. the Campos basin sands, Brazil (Viana et al., 1998a) or the Grand Bank sands, NW Atlantic,

69 offshore Newfoundland (Dalrymple et al., 1992). These could serve as reservoirs (Viana et al., 2007;
70 Viana et al., 1998b).

71 In the Gulf of Cadiz (GoC), a large contourite depositional system (CDS) is present along the Iberian
72 margin due to the Mediterranean Outflow Water (MOW) (García et al., 2009; Hernández-Molina et
73 al., 2006b; Llave et al., 2001; Llave et al., 2006; Stow and Hernández-Molina, 2006). A CDS is the
74 association of various drifts and related erosional features and may vary laterally as well as vertically
75 (Hernàndez-Molina et al., 2008). The GoC CDS has been studied extensively over the past decades as
76 it very large (over 10000 km²), recorded the major changes of the MOW and has an important sand
77 content (Hans Nelson et al., 1993; Hernández-Molina et al., 2006b; Roque et al., 2012; Toucanne et
78 al., 2007). The global interest in this system resulted in IODP Expedition 339 (November 2011-
79 January 2012). This campaign aimed at studying in detail the climatic and oceanographic changes in
80 the Cadiz area and the effect this had on a global scale as well as the distribution of clean and well
81 sorted sand deposits (Expedition 339 scientists, 2012). In contrast to the enormous attention for the
82 northern part, the southern GoC remained largely unstudied up till recently, although a southern
83 branch of the MOW is reported and meddies (Mediterranean eddies) are found in the southern Gulf
84 of Cadiz (Ambar et al., 2008; Richardson et al., 2000).

85 The El Arraiche mud volcano field has been studied extensively in the last decade because of several
86 factors. First, an extensional tectonic regime within a compressional area is present (Flinch, 1993).
87 This results in the presence of extensional ridges (of which the Pen Duick escarpment is one, see Fig.
88 2), characterized by rotated blocks and bound by lystric faults (Van Rensbergen et al., 2005).
89 Secondly, many mud volcanoes (MV, e.g. Gemini MV, see Fig. 2) have been recognized and
90 investigated in the region (Perez-Garcia et al., 2011; Van Rensbergen et al., 2005) and are thought to
91 be the results of subsurface diapirism (Haffert et al., 2013; Perez-Garcia et al., 2011). Mud volcano
92 activity is estimated to have started 2.4 Ma ago (Van Rensbergen et al., 2005) and happened in
93 several phases (Perez-Garcia et al., 2011). Thirdly, the discovery of cold-water corals (CWC) in the

GoC triggered a lot of research (Foubert et al., 2008; Van Rooij et al., 2011; Wienberg et al., 2010). Only a few living CWC are found in the area (De Mol et al., 2011), mostly fossil corals or coral rubble is found (Wienberg et al., 2010; Wienberg et al., 2009). This can be attributed to changing environmental conditions (palaeo-productivity, palaeocanography and change in food supply) which were more favourable during glacial periods in the GoC (Van Rooij et al., 2011; Wienberg et al., 2010). Along the northern east-Atlantic margins (Porcupine, Norway), CWC are thriving nowadays (Frank et al., 2009). Past environmental conditions are difficult to assess as many of the mounds show signs of early diagenesis and are subject to erosion once growth is absent (Foubert et al., 2008; Frank et al., 2009; Templer et al., 2011; Wehrmann et al., 2011). As a consequence, the palaeo-environmental conditions have to be inferred from different parameters. The off-mound history, recorded within drift deposits, may be a good possibility for this.

A small-scale contourite drift is known from the foot of the Pen Duick Escarpment (Fig. 2) (Van Rooij et al., 2011), proposed here to be named the Pen Duick escarpment drift. The position at the foot of the Pen Duick escarpment (Fig. 2) and its location at the foot of several corals mounds make sure this drift is of great interest to the scientific community. This paper attempts to unravel the spatial and temporal evolution of the Pen Duick drift, the involved oceanographic processes and in which way the evolution of the contourite drift was influenced by periods of mud activity. In relation, does the contourite drift contain information on the palaeoceanographic variability of the region and its influence on CWC mound growth?

2. Regional setting

2.1. Geology & geomorphology

The present-day structure and geomorphology of the Gulf of Cadiz is the result of several episodes of rifting, extension and compression from the Triassic onwards (Maldonado et al., 1999; Medialdea et al., 2004). Large allochtonous wedges have been emplaced due to ongoing oblique European-African convergence and the westward motion of the Gibraltar Arc (Middle Miocene), creating the Alboran

119 domain (Maldonado et al., 1999). The sedimentary cover on top of this allochtonous wedge is
120 Neogene in age and is pierced by numerous mud volcanoes (Medialdea et al., 2009; Somoza et al.,
121 2003), salt diapirs (Lolita salt diaper), diapiric ridges (Donana and Cadiz diapiric ridge) and fluid
122 escape features,such as pockmarks (Fig. 1). Most mud volcanoes lie within the offshore Betic-Rifian
123 domain of the accretionary wedge (Medialdea et al., 2004) and are grouped into several fields: the
124 Guadalquivir ridge field, the TAYSO field, the deep Portuguese margin field and the Spanish-
125 Moroccan margin field (Fig. 1). The migration of hydrocarbon fluids towards the surface is facilitated
126 by the presence of many faults and they in turn fuel the mud volcanoes (Pinheiro et al., 2003; Tingay
127 et al., 2003; Van Rensbergen et al., 2005).

128 The Pen Duick Escarpment (PDE) is situated in the southern Gulf of Cadiz, between 35°10'N to
129 35°30'N and 6°30'W to 6°55'W (Figs. 1, 2). It is a part of the Renard Ridge that originated due to the
130 compressive regime in the area, which is in contrast to the extensional regime in the main part of the
131 Gulf of Cadiz (Van Rensbergen et al., 2005). The ridges are bounded by lystric faults (Flinch, 1993)
132 and the compression is estimated to have started 2.4 Ma ago (Van Rensbergen et al., 2005), coeval
133 with the Upper Pliocene Revolution, which marks the onset of the northern hemisphere glaciations
134 and the present-day oceanic circulation (Haq et al., 1987; Hernández-Molina et al., 2002; Lowrie,
135 1986; Maldonado et al., 1999). Seven mud volcanoes are observed in this area, known as the El
136 Arraiche Mud Volcanoe province (Van Rensbergen et al., 2005) and they are part of the Spanish-
137 Moroccan margin field (Fig. 1).

138 CWCs mounds occur on top of Renard Ridge (of which the PDE is a part) (Foubert et al., 2008;
139 Wehrmann et al., 2011) and they from juvenile mounds, like Alpha, Beta and Gamma mound(De Mol
140 et al., 2011; Foubert et al., 2008; Frank et al., 2009). Their occurrence on top of the ridge is the result
141 of both hydrodynamic (currents) and geological (seepage) factors. A three-stage model for CWC
142 mound growth has been proposed by Foubert et al. (2008). First of all, oceanographic, environmental
143 and food-supply conditions need to be right. Wienberg et al. (2010) proved that mound growth

144 prevailed during glacial periods due to enhanced productivity conditions (more Aeolian dust and
145 increased upwelling). Secondly, sedimentation (or the absence of it) becomes important for the
146 mound growth. The supply of food particles and prevention of burial occurs due to increased bottom
147 currents (Van Rooij et al., 2011; Wienberg et al., 2010; Wienberg et al., 2009). Thirdly, diagenetic
148 processes (aragonite dissolution and carbonate precipitation) become important throughout the
149 mound growth (Pirlet et al., 2010). Wehrmann et al. (2011) proved the affection of mounds by
150 ascending methane-bearing fluids, inducing diagenetic processes.

151 Accumulation rates for mound growth as high as 220 cm/ka have been reported during glacials, while
152 during times of reduced mound development (mostly integlacials), only growth rates of 0 to 5 cm/ka
153 have been reported (Frank et al., 2009).

154 **2.2. Oceanography**

155 The oceanography of the northern Gulf of Cadiz is well known due to the presence of the extensively
156 studied contourite depositional system (CDS) originating from the Mediterranean Outflow Water
157 (MOW) (Hernández-Molina et al., 2006b; Llave et al., 2006; Millot, 2009; Stow and Hernández-
158 Molina, 2006). This warm and saline water mass flows out of the Mediterranean Sea via the Gibraltar
159 Strait and continues as an intermediate water mass (500 to 1400 meters water depth) along the
160 Southern Iberian slope due to Coriolis deflection. After its exit out of the Strait of Gibraltar, the MOW
161 is split up into two main branches: the upper and lower Mediterranean waters (García, 2002;
162 Hernández-Molina et al., 2006b). The upper core flows along the shelf edge at depths of 500 to 800
163 meters and the lower core at depths of 750 to 1400 meters to the west-northwest. This last branch
164 splits up into three major branches (from north to south): the intermediate, the principal and the
165 southern branch (Fig. 1) (Louarn and Morin, 2011).

166 On the contrary, the oceanography of the southern Gulf of Cadiz is less studied. In the PDE area (area
167 shown in Fig. 2), 4 water masses are known to occur: the North Atlantic Surface Water (NASW, 0-100
168 m), the North Atlantic Central Water (NACW, 100-600 m), the Antarctic Intermediate Water (AAIW,

600-1500 m) and the North Atlantic Deep Water (NADW, beneath 1500 m) (Ambar et al., 2008; Louarn and Morin, 2011; Machín et al., 2006a). NASW represents the upper 100 meters of the water column and consists of modified NACW. NACW is characterized by a linear decrease in temperature (16°-12°C) and salinity (36.25-35.5) (Criado-Aldeanueva et al., 2006; Louarn and Morin, 2011) and flows from west to east in the Gulf of Cadiz. NACW splits up in the Gulf of Cadiz: it recirculates southwards along the African coast due to deflection of a coastal upwelling zone, northwards along the Iberian margin and another branch flows directly into the Mediterranean Sea (Fig. 1) (Machín et al., 2006b). The general circulation pattern of the these upper two water masses is anticyclonic, as they are part of the Azores current, which is in turn part of the northeastern Atlantic circulation (Machín et al., 2006a). AAIW is characterized by low oxygen and high silicate values. Although intensive mixing with under- and overlying water masses makes its direct recognition problematic, AAIW is known to flow northwards along the African coast in the southern Gulf of Cadiz, before being outcompeted in the north by MOW. Salinity values of AAIW (35.6) are slightly higher than the values of the lower NACW (35.45) (Louarn and Morin, 2011). NADW is present below 1500 meters and flows from south to north in the Gulf of Cadiz (Fig. 1), along the Atlantic margin. It is characterized by low salinities (<35.5) and temperatures (<8°C) (Louarn and Morin, 2011).

The PDE experiences the influence of NACW at its top (550 meters water depth) and AAIW at its foot (650 meters water depth, Fig. 3) (Van Rooij et al., 2011). At present, MOW does not occur along the PDE, as Mediterranean waters are not observed above 700 meters water depth (Fig. 3) (Mienis et al., 2012) and CTD data do not indicate their presence (Van Rooij et al., 2011) (Fig. 3). However, meddies are known to transport MOW south of the Strait of Gibraltar (Fig. 3) (Ambar et al., 2008; Richardson et al., 2000) and the MOW is strongly influenced by glacial-interglacial alternations, with a stronger MOW during glacial periods (Toucanne et al., 2007). So, the influence of the MOW in the region cannot be excluded, certainly as Van Rooij et al. (2011) and Foubert et al. (2008) inferred the possibility of an intensified glacial MOW, being able to reach the PDE through enhanced meddy activity.

195 **3. Material and methods**

196 Within the framework of the R/ V Belgica “CADIPOR” cruises (2001, 2005 and 2007) and the “Pen
197 Duick” campaign (2009) in the southern GoC, a total of 520 km high-resolution single channel seismic
198 sparker profiles have been acquired at the foot of the Pen Duick escarpment and the Gemini mud
199 volcano. A SIG sparker (80 electrodes in 2001, 120 electrodes in 2005, 2007 and 2009) has been used,
200 with a shot interval of 2 seconds (3 seconds in 2009). The energies reached 500 J and a 8 kHz
201 sampling frequency has been used. A record length of 1.6 s TWT (in 2001), 1.8 s TWT (in 2005 and
202 2007) and 2.5 s TWT (in 2009) was obtained. The profiles were acquired with acquisition velocities
203 within the range of 3 to 4 knots.

204 The profiles (Figs. 5, 6 and 7) have been processed using the DECO Geophysical RadexPro processing
205 software. A swell filter, bandpass filter (Butterworth type, low cut at 200 Hz, low-cut slope of 24 dB/s
206 and high cut at 1500 Hz, high-cut slope of 36 dB/s), predictive deconvolution, 2D spike removal and
207 amplitude corrections have been applied.

208 The multibeam data (in total 700 km²), recorded during the CADIPOR I cruise (2001) have been
209 obtained using the SIMRAD EM1002 system, extended with a deep water module, permanently
210 installed on R/V Belgica. The swath width was 500 meter above 500 meters water depth and 750
211 meters below. The data have been corrected and cleaned using Kongsberg’s Merlin and Neptune
212 packages. The footprint at 400 meters water depth is 15x15 meters. This dataset was already
213 extensively described with respect to the main geomorphological features and mud volcanoes within
214 Van Rensbergen et al. (2005).

215 Profile M2005_105 (Fig. 4) has been acquired by the R/V Pelagia in 2006 within the framework of the
216 ESF EuroDIVERSITY MiCROSYSTEMS project. Three airguns (10, 20 and 40 cubic inch volume) were
217 used and they were towed in a frame at 1.3, 1.8 and 2.0 meters depth. The guns were towed 37
218 meters behind the stern of the ship and fired every 5 seconds at a pressure of 100 bars, resulting in
219 an average distance between the shots of 10.5 meters (4.2 knots sailing speed). The streamer (towed

at a depth of 1 meter below surface) consists of four 63 meter long sections with 6 channels each. Each channel has 10 Teledyne T2 hydrophones (interval of 1 m). The data were recorded by the Geo-Resources Geo-Trace 24 hard- and software system, consisting of a 24 channel digital pre-amplification system. The record length was 2000 ms TWT and the sampling interval 0.5 ms. When recording, a bandpass filter (30 Hz high pass and 700 low pass) was applied. On board, the lines were stacked and preliminary migration has been performed.

4. Results

4.1 Geomorphology

The study area extends from 35° 22' N to 35° 14'N and 6° 52' W to 6° 45' W (Fig. 2). Within the investigated area, the multibeam data show the presence of the PDE (about 80-100 meters above the seafloor), three mud volcanoes (e.g. Gemini MV, about 150 meters high), CWC mounds (on top of the PDE, previously discussed by amongst others De Mol et al. (2011) and Templer et al. (2011)) and 6 mounded structures along the foot of the PDE. They have a diameter between 200 and 300 meters and are between 5 and 10 meters high.

A semi-continuous channel, with widths varying between 200 and 300 meters, is present along the foot of the aforementioned topographies (Fig. 2). The channel is about 10 km long from its most southeastern (along Gemini mud volcano) till its most northwestern (northern boundary PDE) expression. The first 2 km of this channel have an east-west direction, following the southern border of the Gemini MV. Here, the most pronounced expression of the channel is observed with depths differences up to 15 m (see inset Fig. 2). Then, it changes to a south-southeast to north-northwest direction for 8 km, following the base of the Gemini MV and PDE, respectively. When the channel passes the boundary between the Gemini MV and the PDE, the depth decreases strongly (to about 5 m) and increases again along the PDE. Along the PDE, the depth of the channel varies between 5 and 15 m, with a gradual decrease in expression towards the first of the six mounds. Along these mounds, two channels are observed: one which continues along the foot of the PDE and increases in depth, to

245 former values of about 15 m and a second one WSW of the mounds (depths of about 15 m). Both
246 gradually lose their expression to the northwest.

247 Immediately south (along the Gemini MV) or southwest (along the PDE) of the channel, mounded
248 sediments are present. They rise about 3 to 5 m above the smoothly dipping (about 1° SW) seafloor
249 south (-west) of them and 5 to 20 m above the base of the channel (see inset Fig. 2).

250 **4.2 Seismic stratigraphy**

251 Based on the seismic sparker profiles and the multichannel airgun profile, 5 seismic stratigraphic
252 units have been discerned, separated by 4 discontinuities D1 to D4. Due to the lower penetration of
253 the sparker source (about 400 ms TWT, while at least 800 ms TWT for the airgun), only 4 of the 5
254 units are visible on the high-frequency sparker profiles. The PDE and Gemini MV can be considered as
255 the acoustic basement in the ENE, but in the WSW, no real acoustic basement is observed. This due
256 to attenuation of the signal in the thick sedimentary package. Reflectors can be distinguished in the
257 sparker profiles up to depths of about 1200 ms TWT (Figs. 5,6,7) and down to 1700 ms TWT in the
258 airgun profile (Fig. 4). Below this depth, the multiple inhibits its further recognition. Fig. 4 shows that
259 (semi-) continuous deposits of units 1 to 5 are bounded by the PDE or Gemini MV in the northeast
260 and a palaeohigh in the southwest. In the southwest, the palaeohigh rises to 150 to 200 ms beneath
261 the seafloor (Fig. 4). The seismic facies of the palaeohigh consists of very chaotic, discontinuous
262 reflectors of varying intensity. This facies differs from the seismic facies within the mud volcanoes in
263 the fact that the palaeohigh still contains reflections, while the mud volcanoes and tectonic ridges
264 have an almost acoustically transparent facies (Fig. 5, 6 and 7).

265 4.2.1 Unit 1

266 Unit 1 (only visible on Fig. 4) consists of low-amplitude semi-continuous reflectors at the base and
267 more continuous, slighter higher amplitude reflectors at the top. In the southwest, the unit is
268 intersected with many normal faults (see below). Unit 1 displays a more low-angle onlap onto the

basement in the east, while in the west a higher angle of onlap onto the palaeohigh is encountered (Fig. 4). In Fig. 4, the top of the unit is incised deeply (± 60 ms TWT) along the Gemini MV. Thicknesses of unit 1 vary between 150 ms TWT in the west-southwest and up to 550 ms TWT in the middle of the basin. The maximum thickness cannot be calculated, as the multiple inhibits the observation of the lower boundary (Fig. 4).

Unit 1 and a small part of unit 2 are affected by 2 distinct fault patterns: one major fault is located in the centre of the basin and at least nine smaller ones to the west-southwest (Fig. 4). The large fault (about 750 meters long and a dip of about 50-55°) is a normal, east-up fault with offsets of 10 ms TWT at its top (about 1250 ms TWT), going to zero offsets at 1450 ms TWT. Deeper down, the offset cannot be determined anymore due to a chaotic seismic expression. The smaller faults are normal, east-up faults as well and all have offsets inferior to 5 ms TWT. Activity along the faults stop within the lower part of Unit 2.

4.2.2. Unit 2

The boundary between units 1 and 2 is erosive, evidenced by the incision into unit 1 along the Gemini MV (Fig. 4). Unit 2 consists of low to medium-amplitude, continuous reflectors at the base and medium-amplitude, continuous reflectors at the top (Figs 5, 6). Overall, slightly mounded deposits are present in this unit, observable about 500 meters SSW of the PDE and Gemini MV (Figs. 5, 6). Unit 2 fills a small incision at the intersection along the Gemini MV, showing a gradual decline in incision upwards (only visible on Fig. 4). The base of the incision contains discontinuous, slightly chaotic deposits, while more continuous deposits arise on top. Eight small cyclic subunits, each one about 25 to 35 ms TWT thick (Figs. 5, 6) are observed within this unit. Subunit c has slightly higher amplitude deposits, compared to the other 7 subunits. All subunits display very high amplitude reflectors at their base and lower amplitudes on top. Along the PDE, the subunits are conform and pinch-out of the reflectors is observed (Fig. 6), evidenced by the rise of individual reflectors (a concave appearance) and a decrease in thickness of the subunits towards the PDE. The pinch-out is

294 greatest at the base of unit 2 and gradually diminishes upwards, nearly being absent at the top of
295 unit 2. Along the Gemini MV, a different pattern is observed: the subunits display small erosional
296 features. At the base of unit 2, first evidence of a Christmas-tree structure appears (Fig. 5). This
297 pattern of mud extrusions disrupts the sedimentation at the foot of the Gemini MV and can be
298 observed in all other units as well. The reflectors on top of these extrusions display a convex pattern
299 and gradually even out the extrusions (Fig. 5). Unit 2 is still faulted at its base, but the small
300 depression, left by the large fault, is gradually being evened out in this unit (Figs 4, 6). Thicknesses
301 vary between 200 and 250 ms TWT for most of the unit with a gradual decrease towards the
302 northwest (Fig. 8). In the west-southwest, thicknesses are reduced due to the presence of the
303 palaeohigh (Figs. 4, 8).

304 4.2.3. Unit 3

305 Units 2 and 3 are separated by an angular unconformity. Small-scale erosion has occurred along both
306 PDE and Gemini MV and the accommodation space is filled up by deposits of Unit 3 (Figs. 5, 6). Unit 3
307 has low-amplitude reflectors at its base and moderate-amplitude ones at its top along most of the
308 PDE (Fig. 6) and consists of mostly high-amplitude reflectors with a low-amplitude part in the middle
309 along the Gemini MV (Fig. 5). Four subunits have been discerned in this unit. The difference in
310 amplitudes of the different subunits is low (although some high-amplitude reflectors are present)
311 and they are distinguishable based on small angular unconformities (visible along both topographies,
312 Figs. 5, 6). A channel is present along the Gemini MV and a large part of the PDE with mounded
313 sediments on its south-western side. The channel is about 150 meters wide and incisions increase
314 upwards (5 ms TWT to 20 ms TWT). More erosion occurred along the PDE, as incisions are deeper
315 (Figs 5, 6).

316 Along the most northern part of the PDE, the unit has a different appearance: very high amplitudes
317 at the base, moderate in the middle and high again at the top (Fig. 7). Also, no evidence for a channel
318 along the PDE is observed here: the sedimentation pattern is obscured due to the presence of one of

the mounds and the resulting diffraction hyperbola. But what really sets it apart in this area is the occurrence of 3 big and 2 small mounded structures within this unit (Fig. 7). They have an acoustically almost transparent appearance. The two small ones (a few ms TWT high and less than 20 meters wide) are situated deeper compared to the big ones (Fig. 7). The tree big mounded structures (between 20 and 30 ms TWT high and between 100 and 250 meters wide) originate at the same stratigraphic level, depending on the position of the mound 15 to 25 ms TWT above the base of Unit 3 (Fig. 7). The sediments deposited on top display a concave appearance because of their presence.

Thicknesses are fairly constant and vary around 100 ms TWT, only along the mounds, 70 ms TWT of sediment is present (Fig. 8). Slightly reduced values when approaching the PDE or Gemini MV (a decrease of about 20 ms TWT) are observed as well (Fig. 8).

4.2.4 Unit 4

The boundary between units 3 and 4 (D3) is the most erosive one of the entire sedimentary sequence. Along the PDE and Gemini MV, up to 25 ms TWT of sediments of Unit 3 are eroded by the discontinuity, creating a channel with the same incision depth. The channel, which is present throughout the entire unit, is filled differently along the PDE and Gemini MV (Figs. 5, 6). Along the Gemini MV, continuous high-amplitude reflectors are encountered within the channel. They all have a concave appearance (moat and mounded sediments) due to the continuing presence of a channel (Fig. 5). Along the PDE, a heart-shaped block of chaotic and nearly reflection-free deposits is encountered within the channel. This block has a small run-out and is up to 50 ms TWT thick and 300 meters long. Fig. 8 shows the position of these deposits. In the rest of the unit, high-amplitude, nearly horizontal, continuous deposits are present (Figs. 5, 6).

Based on small erosional surfaces and changes in acoustic appearance, 3 subunits have been discerned within Unit 4. The lowermost subunit (15-20 ms TWT thick) contains lower amplitudes compared to the upper two (Figs. 5, 6). Within the upper subunit, along the PDE, a channel (about 100 meters wide and only a few ms TWT deep) is observed about 750 meters southwest of the PDE

(Fig. 6). Due to the thinning of this unit towards the north (Fig. 8), the subunits were no longer discernable in Fig. 7. Unit 4 is the thinnest of the sedimentary sequence with values varying around 50 ms TWT (Fig. 8). At the position of the heart-shaped block, thicknesses go to zero.

4.2.5. Unit 5

A partly erosive boundary separates Units 4 and 5, although it is less erosive compared to the previous discontinuity. Along the Gemini MV, at the boundary between Units 4 and 5, a large concave extrusion (up to 800 meters wide and 40 ms TWT deep) is observed (Fig. 5). A channel is present along the PDE and Gemini MV, although the appearance is different. Along the Gemini MV, the channel is very wide (about 800 meters and 20 ms TWT deep) at the base. During deposition of the upper subunit (5c), incision into the underlying deposits along the mud volcano is observed (Fig. 5). Along the PDE, a small channel (200 meters wide and 10 ms TWT deep) is present SSW of the heart-shaped deposits within the lower two subunits (5a and b). Within the upper subunit (5c), a wide channel (about 1 km wide and about 25 ms TWT deep) is present along the PDE (Fig. 6). Along the northern part of the PDE, a second channel has developed just southwest of the mounds at the base of the PDE. This channel is 150 meters wide and up to 15 ms TWT deep. Southwest of this second channel, mounded sediments are observed which pass into conformable deposits. In total, 3 subunits have been discerned based on small angular unconformities. All subunits consist of high amplitude, continuous reflectors. In Fig. 7, the subunits were again not discernable due to the decreases thickness (Fig. 8). Thicknesses are slighter bigger than unit 4: on average 50 to 55 ms TWT (Fig.8). The mound displays remarkable seismic features: its WSW side contains chaotic, very low-amplitude reflections, while its ENE side displays short horizontal, continuous reflections which seem to be a prolongation of the underlying sedimentation.

5. Discussion

5.1 Sedimentary processes

5.1.1 Initiation (Unit 1)

The deposits of Unit 1 drape the basin-boundary and gently level the deepest regions. Settling of sedimentary particles in absence of strong currents, resulting in (hemi-)pelagic deposits (depending on the amount of biogenic material), is proposed as the depositional mechanism. Unit 1 and the base of Unit 2 are affected by faults: several smaller faults at the flanks of the palaeohigh and a large normal fault in the middle of the basin. This faults may be due to the compressional regime in the region (Van Rensbergen et al., 2005). However, as there is only one profile showing these features, they cannot be mapped and as a consequence, the real orientation and direction cannot be derived. The palaeohigh resembles the compressional tectonic ridges (Vernadsky, Renard) and may also be a compressional ridge that did not reach the seafloor and is covered by sediments as a consequence.

5.1.2 Sheeted drift (Unit 2)

From Unit 2 onwards, very gradually, a contourite drift is being constructed, perpendicular to the margin, with sheeted and detached mounded drift deposits.

Unit 2 mostly consists of horizontal, continuous, slightly mounded deposits. Only along the northern part of the PDE, the mounded nature is absent. This mounded nature increases towards the top of the unit (Figs. 5, 6) and indicates together with the fairly uniform thickness perpendicular to the PDE and Gemini MV (Fig. 8), the aggradational stacking pattern and the location along a steep slope towards slope sheeted drift deposits (Faugères and Stow, 2008). Theoretically, sheeted drifts are associated to velocities below 10 cm/s (Stow et al., 2008). The presence of pinched deposits, onlapping onto the PDE within the entire unit suggests a syn-lift sedimentation, affected by the uplift of the PDE, as suggested by Van Rooij et al. (2011). This process diminishes the thickness of the unit in this part of the drift (Figs. 6, 8). The pinch-out diminishes towards the top of the unit and is absent above D2, meaning that the uplift of the PDE stopped at D2. This is not the case near Gemini MV, where a Christmas-tree structure is present, protruding into most of the units (2 to 5), similar to profiles presented in Praeg et al. (2009), Somoza et al. (2003) and Somoza et al. (2012). Periodic mud

393 extrusion from the mud volcano is responsible for this phenomenon, with the largest mud intrusion
394 observed within the upper part of Unit 4 (Fig. 5). After the extrusions, the Pen Duick drift covers the
395 mud with concave deposits (Fig. 5).

396 5.1.3 Mounded drift: Units 3-5

397 Within the sedimentary sequence, the most striking change is the evolution from horizontal, slightly
398 mounded (and along the PDE pinched-out) deposits (Unit 2) into upslope prograding, mounded
399 deposits with a moat (the observed channel) along the PDE and Gemini MV (Units 3 to 5, Figs. 5, 6).
400 Mounded drifts are associated to velocities between 10 and 30 cm/s (Stow et al., 2008), meaning
401 that the inferred bottom current velocities are higher than those present during the deposition of
402 Unit 2. The bottom current strength also increases during the deposition of Unit 3, especially along
403 the southern part of the PDE as the depth of the moat (5 to 20 ms TWT) and the expression of the
404 associated sediment drift mound increases (Figs. 5, 6). This can be interpreted as the evolution from
405 the initiation of mounded drifts towards a continuous bottom current intensity within the moat,
406 gradually leading to erosive (upper parts of Unit 3) instead of non-depositional action (lower parts of
407 Unit 3). Along the northern part of the PDE, a moat and mounded sediments are absent and (hemi-)
408 pelagic sedimentation is present (Fig. 7). This can be interpreted as a lateral decline in bottom
409 current strength, which in this region are not able to create drift deposits. The decline in thickness of
410 Unit 3 (Fig. 8) from southeast to northwest illustrates the lateral change in sedimentation pattern:
411 mounded drift deposits are thicker and occur in the southeastern part and pelagic sediments are
412 thinner and occur in the northwest.

413 Three mound-like structures, originating at the same stratigraphic level, have been observed within
414 Unit 3 in Figure 7. They closely resemble buried CWC mounds discussed by Huvenne et al. (2003),
415 Iacono et al. (accepted) and van Weering et al. (2003) and are classified as such as a consequence.
416 The occurrence of CWC mounds in this part of the study area implies that environmental conditions

(food supply, prevention to burial) were right during at least a certain amount of time for CWC to flourish (Foubert et al., 2008; Wienberg et al., 2010; Wienberg et al., 2009).

An erosive boundary separates Units 3 and 4 (Figs. 6, 7). Unit 4 is characterized by a larger (and along Gemini MV wider) moat, except for the northern part of the PDE. In this area, the moat is still absent, indicating the continuing lateral decline in bottom current intensity. The erosive nature of the moat indicates faster bottom currents, capable of eroding more sediment. The wider moat along the Gemini MV might indicate a less focussed bottom current. A large mud extrusion is observed at the base of subunit 4c (Fig. 5). This has the same seismic characteristics as and is positioned at the same stratigraphic level as the triangular deposits in Fig. 6. The similarities between both and its position near the Gemini MV indicate a muddy origin for the triangular deposits as well, extruded at the same period. The separate patches of mud (Fig. 2) can be due to two different pathways, certainly as Gemini MV actually consists of two mud volcanoes within one mud cone (Van Rensbergen et al., 2005). The thickness maps (Fig. 8) clearly show the position of the mud extrusion. After the large mud extrusion, the depocenter shifted SSW-wards, hinted by the relocation (about 500 meters) of the moat and mounded sediments (Figs. 5, 6). Along the Gemini MV, this relocation only happens at the base of Unit 5, along the PDE this happens already within subunit 4c.

Unit 5 consists of elongate mounded drift deposits along both topographies, even along the northern part of the PDE (Figs.5, 6 and 7). This indicates focussed bottom currents along the entire PDE, strong enough to create drift deposits. A broad and deep moat is present during the deposition of Unit 5. Along the Gemini MV, the moat is at its widest (about 500 meters) of the entire Pen Duick drift, which hints towards a less focussed bottom current, compared to previous units (Fig. 5). Only within the present seafloor, a narrow, deep moat is present directly SSW of the Gemini MV again and is accompanied by a shift in depocenter (Fig. 5). Along the PDE, a narrow but deep moat is present about 500 meters SSW of the escarpment (Fig. 6). Also here, within the present seafloor, the position of the moat shifted to the foot of the PDE.

442 The occurrence of semi-buried CWC mound, recognized at the base of the northern part of the PDE,
443 is a most peculiar feature (Fig. 7). In morphology (width, height, shape) they resemble the CWC
444 mounds found on top of the PDE (Foubert et al., 2008; Van Rooij et al., 2011). However, the presence
445 of continuous reflectors facing the PDE side of these mounded features, resembling the
446 sedimentation below, contradicts a 100% CWC origin. Given the fact that the WSW part of the
447 mound contains a seismic facies resembling the buried mounds of Unit 3 (Fig. 7) and the ENE part
448 contains continuous, parallel, horizontal reflectors, a dual origin for the mounds is proposed. CWC
449 started to settle at the base of the PDE and initiated mound growth. They build a mound against
450 which sediment was deposited, provided by the bottom current along the PDE (inset Fig. 9). This
451 created the mounds, consisting of both a sedimentary (ENE) and CWC mound (WSW) part. This
452 implies that conditions for CWC to thrive were favourable at the foot of the PDE in this region.
453 Unfortunately, further investigations are required to further reveal and understand the exact nature
454 and origin of these features. A small moat along the WSW part of the mounds implies a bottom
455 current flowing along them. Probably due to the presence of these mounds, the depocentre shifted
456 to the WSW and separated mounded drift deposits are present to the WSW (Fig. 7). Whether the
457 bottom current flowing along the Gemini MV and PDE splits or a second bottom current, unrelated to
458 the first one, is present cannot be derived from these profiles (Fig. 2).

459 **5.2 Chronostratigraphy**

460 The spatial and temporal distribution of the Pen Duick contourite drift indicates a depositional
461 history including several changes in sedimentation patterns. Two major (D1, D2) and two minor
462 transitions (D3, D4) are recorded as unconformities separating the depositional sequences. D1 is
463 initiation of drift deposit, D2 marks the transition from sheeted to elongated mounded drifts,
464 whereas D3 and D4 indicate changes within the elongated mounded drift deposits. These alterations
465 have been compared to surrounding regions in order to derive a possible chronostratigraphy. Maad
466 et al. (2010) discussed the seismic stratigraphy of the northwestern Moroccan Atlantic continental

shelf based on sparker seismic data. Their unit Q2 is considered to have a Middle to Upper Pleistocene age (correlation with well LAR-A1, 25 km east-southeast of the research area). Correlation (through connecting seismic profiles) of this unit to the investigated region reveals that at least units 3, 4 and 5 are within that age range.

Petrographic studies of mud breccia clasts show that the Al Idrissi mud volcano field is situated on an Upper Miocene-Pliocene sedimentary basin (Akhmanov et al., 2003; Pinheiro et al., 2003), implying that the sedimentary deposits described in this paper are of Plio-Pleistocene age. The mud volcanoes appeared 2.4 Ma ago (Van Rensbergen et al., 2005) or 2.6 Ma according to Perez-Garcia et al. (2011), implying that the entire contourite drift (Units 2 to 5) is post-Pliocene in age and only Unit 1 has a possible Pliocene age. Moreover, the basal unconformity, discussed by Van Rensbergen et al. (2005) and Perez-Garcia et al. (2011), is set at an age of 2.6 Ma and agrees to D1. This means that discontinuity D1 could be associated to the BQD (base Quaternary discontinuity), set at 2.588 Ma (Gibbard et al., 2010).

During the Quaternary, the Middle Pleistocene Revolution is the most important oceanographic change in the Gulf of Cadiz (and by extension, the entire North-Atlantic), coeval with the switch to a "full" glacial mode with 100 ky eccentricity cyclicity (Cacho et al., 2000; Frigola et al., 2008; Hernández-Molina et al., 2011; Llave et al., 2007; Llave et al., 2006). Changes in water mass circulation and marine sedimentation patterns, mostly evidenced by higher amplitude reflectors and more vigorous current patterns, are observed in the Gulf of Cadiz (Hernández-Molina et al., 2006b; Llave et al., 2007), the Cantabrian margin (Van Rooij et al., 2010) and the Porcupine Seabight (Van Rooij et al., 2007). A similar observation has been made here: a switch from sheeted to elongate mounded drift deposits and a gradual increase in amplitudes of the reflections throughout Units 3, 4 and 5 (Figs. 5, 6, 7). Therefore, discontinuity D2 may be correlated to the MPR (0.920 Ma).

Continental shelves and upper slopes are more prone to eustatic variations compared to deep-water environments and in response, bottom currents fluctuate more in these regions (Hernández-Molina

et al., 2002; Ridente et al., 2009; Verdicchio and Trincardi, 2008). The upper three units display features which can be attributed to climatic variations: a cyclic pattern of progradational (onto the PDE or Gemini MV) subunits with reflectors of varying amplitudes. As the majority (65-80%) of the sediment is deposited during regressive and lowstand periods in the Gulf of Cadiz and the Alboran Sea (Hernández-Molina et al., 2002), the subunits can be tentatively linked to glacial marine isotopic stages (MIS). This correlation has been applied before along the Adriatic margin by Ridente et al. (2009) and along the southwestern Mallorca shelf by Vandorpe et al. (2011). The ten discerned subunits from the MPR to Recent can be correlated to the ten (even) MIS (Lisiecki and Raymo, 2005) (Figs. 5, 6). A periodicity of 80 to 120 ky is obtained due to this correlation, which is in agreement with the obliquity pacing hypothesis proposed by Huybers and Wunsch (2005) and Huybers (2007), stating that glacial cycles vary by 80 or 120 ky in the late-Pleistocene by skipping one or two obliquity beats. As a result, D3 and D4 are linked to MIS 15 (about 575 ka) and 9 (about 325 ka) respectively. At 575 ka, an intensification of the bottom current regime occured in the area, evidenced by larger moat (Figs. 5, 6). At 325 ka, a defocussing occurred, leading to a wider, less deep moat (Figs. 5, 6).

Based on this chronostratigraphy and the average measured thicknesses (conversion into meters based on a theoretical seismic velocity of 1650 m/s within the sediment), the sedimentation rate for the period between BQD and MPR (Unit 2) is 10.8 cm/ky and between MPR and Recent (Units 3 to 5) 17.0 cm/ky. These rates are close to or within the range of theoretical values for sediment drifts: 3-10 cm/ky for sheeted drifts (Unit 2) and 5-30 cm/ky for mounded drifts (Units 3 to 5) (Stow et al., 2008). Also, the increase in sedimentation rate after the MPR is consistent with the enhanced sedimentation rates observed in the Cadiz CDS in the north (Llave et al., 2001; Llave et al., 2011) and the Le Danois CDS (Van Rooij et al., 2010).

5.3 Comparison to the northern Gulf of Cadiz palaeoceanography

When comparing the depositional history of the Pen Duick contourite drift to other systems along the eastern boundary of the North Atlantic (Cadiz and Le Danois CDS), several resemblances and

differences can be identified. While in the Cadiz and Le Danois CDS, drift deposits are present from the Pliocene onwards, the PDE area only contains Quaternary drift deposits. After the MPR, an intensification of bottom currents and an accompanying growth of the CDS occurs in all drift systems, expressed by a severe growth phase of the mounded drift deposits in the Cadiz and Le Danois areas (Llave et al., 2011; Roque et al., 2012; Van Rooij et al., 2010) and by the evolution from sheeted to mounded drift deposits in the PDE area (Figs. 5, 6). A final intensification stage is observed in the Cadiz CDS around MIS 12 (Llave et al., 2001; Llave et al., 2007; Llave et al., 2011; Marchès et al., 2010; Roque et al., 2012), while in the Pen Duick drift, this intensification is tentatively set at MIS 15. The boundary at MIS 9 observed in the Pen Duick drift is not encountered in the other systems.

The vast differences in evolution between MOW-controlled CDS's and the Pen Duick contourite drift indicates that MOW is not likely to be involved in the formation or shaping of the Pen Duick drift. Although the MOW is present within the area as meddies (Ambar et al., 2008), along the PDE it is not observed (Only in deeper water settings, Fig. 3). During glacial periods, MOW flows at even greater depths (García et al., 2009) and therefor, its presence at the foot is of the PDE during glacials is not likely as well. AAIW enters the Gulf of Cadiz in the south and flows along the African coast towards the north, before being outcompeted by the MOW (Louarn and Morin, 2011; Machín et al., 2006a). CTD data from Van Rooij et al. (2011) and Mienis et al. (2012) indicate the presence of AAIW at the foot of the escarpment, while NACW is present on top. The absence of MOW, the proved presence of AAIW and the depth range in which the Pen Duick drift occurs favours towards an AAIW-origin and would make it the most northern contourite drift in the Atlantic Ocean with a possible AAIW-origin.

Mienis et al. (2012) showed the presence of northeast-directed currents at the foot of the PDE. This is in agreement with the observed seismic characteristics and geomorphology of the Pen Duick drift. A moat is present along the PDE and Gemini MV, indicating a bottom current along both topographies. This bottom current has been active throughout the entire Quaternary (Figs. 5, 6 and 7), depositing sediment SSW of the Gemini MV and PDE. Taking into account the pathway of the

542 bottom current and the Coriolis deflection to the right in the northern hemisphere, the bottom
543 current is inferred to have an northeastward direction. The pathway of the AAIW, the CTD data and
544 the flow direction at the foot of the topographies together hint towards a bottom current coming
545 from the south (most likely an AAIW-origin), being deflected by the Gemini MV and PDE and which
546 continues to flow along the bases of the topographies due to Coriolis deflection. The start of drift
547 formation (Unit 2, Figs. 5, 6) 2.588 Ma ago coincides with the first signs of mud eruption and the
548 initial uplift of the PDE (Perez-Garcia et al., 2011; Van Rensbergen et al., 2005). So, only when the
549 Gemini MV and PDE rose high enough to alter the bottom current pattern and possible speed them
550 up (Faugères et al., 1999), the Pen Duick contourite drift started to form. Higher velocities due to
551 small-scale topographies (such as seamounts, mud volcanoes, escarpments, …) are commonly
552 described (Hernández-Molina et al., 2011; Rebesco et al., submitted; Stow et al., 2009). Taking into
553 account the fact that bottom currents are on average 8 cm/s on the plain at the foot of the PDE
554 (Mienis et al., 2012) and that drift deposits solely occur along the topographies, the Pen Duick
555 contourite drift is an excellent example of an obstacle-related contourite system.

556 **6. Conclusions**

557 Based on sparker single-channel seismic, an airgun multi-channel seismic and multibeam data, a
558 contourite drift along the southwestern border of the Pen Duick escarpment and Gemini mud
559 volcano has been described in terms of sedimentary evolution and palaeoceanography. Five
560 conclusions can be drawn from this study:

561 1. The Pen Duick contourite drift is an excellent example of an obstacle-related drift as it occurs in
562 an area with in general low bottom-currents. Bottom currents are deflected against the
563 topographies (PDE and Gemini MV) and build a contourite drift along them, perpendicular to the
564 continental margin.
565 2. The Pen Duick contourite drift originates at the base of the Quaternary, creating sheeted drift
566 deposits (Unit 2). Bottom currents intensify after the MPR, leading to the deposition of separated

mounded drift deposits (Unit 3 to 5). A general intensification of bottom currents is inferred from the MPR to present

3. The presence of the Gemini MV interferes with the drift deposits: several extrusions are recorded within the sedimentary sequence leading to a Christmas-tree structure along the mud volcano. The presence of a large block of mud along both PDE and Gemini MV within unit 4 indicates a large eruption in that period.
4. The Pen Duick contourite drift has a possible AAIW-origin which makes would make it the most northern expression of AAIW within the Atlantic Ocean. Evidence (both seismic and CTD) for the presence of MOW at the foot of the PDE is not present.
5. CWC mounds have been found within and on top of the northern part of the Pen Duick drift. This means that not only on top of the PDE, environmental conditions were right for CWC to flourish, but also at its base. The presence of the buried mounds indicates that also in the past, conditions were favourable for CWC mound growth.

7. Acknowledgments

The authors would like to acknowledge the captains and crews of R/V Belgica and R/V Pelagia for the many successful cruises to the study area. The helpful and stimulating discussions with J.-P. Henriet (UGent) and F.J. Hernández-Molina (U. Vigo) are greatly appreciated. The data was acquired within the framework of the following past projects: ESF EuroDIVERSITY MiCROSYSTEMS, ESF EuroMARGINS MoundForce, EC FP6 HERMES (GOCE-CT-2005-511234) and EC FP7 IP HERMIONE (Grant agreement n°226354). The aims and strategies of this paper were elaborated within the framework of the FWO-Flanders project “CONTOURITE-3D”, as well as IGCP project 619 and INQUA project 1204. Finally, we wish to thank the reviewers for their helpful comments.

8. References

World Ocean Database, 05/02/2013. http://www.nodc.noaa.gov/OC5/WOD09/pr_wod09.html.

592 Akhmanov, G., Ivanov, M., Henriet, J.P., Sarantzev, E.S., 2003. The El Arraiche mud volcano field and
593 its "exotic" mud volcano deposits recovere during the TTR-12 cruise in the Gulf of Cadiz, in: Marani,
594 M., Akhmanov, G., Suzyumov, A. (Eds.), Geological and biological processes at deep-sea European
595 margins and oceanic basins. UNESCO, Bologna, Italy, pp. 9-10.
596
597 Ambar, I., Serra, N., Neves, F., Ferreira, T., 2008. Observations of the Mediterranean Undercurrent
598 and eddies in the Gulf of Cadiz during 2001. Journal of Marine Systems 71, 195-220.
599
600 Antich, N., Buitrago, J., García Mojonero, C., Jiménez, A., Martínez del Olmo, W., 2005. Contourites:
601 An unknown and excellent reservoir (Gulf of Cadiz, SW Spain). 25 aniversario de la Asociación de
602 Geólogos Geofisicos Españoles del Petróleo AAGGEP, Spec. Publ., 75-82.
603
604 Cacho, I., Grimalt, J.O., Sierro, F.J., Shackleton, N., Canals, M., 2000. Evidence for enhanced
605 Mediterranean thermohaline circulation during rapid climatic coolings. Earth and Planetary Science
606 Letters 183, 417-429.
607
608 Criado-Aldeanueva, F., García-Lafuente, J., Vargas, J.M., Del Río, J., Vázquez, A., Reul, A., Sánchez, A.,
609 2006. Distribution and circulation of water masses in the Gulf of Cadiz from in situ observations.
610 Deep Sea Research Part II: Topical Studies in Oceanography 53, 1144-1160.
611
612 Dalrymple, R.W., LeGresley, E.M., Fader, G.B.J., Petrie, B.D., 1992. The western Grand Banks of
613 Newfoundland: Transgressive Holocene sedimentation under the combined influence of waves and
614 currents. Marine Geology 105, 95-118.
615

De Mol, L., Hilário, A., Van Rooij, D., Henriet, J.P., 2011. Habitat mapping of a cold-water coral mound on Pen Duick escarpment (Gulf of Cadiz), in: harris, P., Baker, E. (Eds.), Seafloor morphology as benthic habitat. Elsevier, pp. 645-654.

Duarte, C.S.L., Viana, A.R., 2007. Santos Drift System: stratigraphic organization and implications for late Cenozoic palaeocirculation in the Santos Basin, SW Atlantic Ocean. Geological Society, London, Special Publications 276, 171-198.

Expedition 339 Scientists, 2012. Mediterranean outflow: environmental significance of the Mediterranean Outflow Water and its global implications. *IODP Prel. Rept.*, 339. doi:10.2204/ iodp.pr.339.2012

Faugères, J.-C., Stow, D.A.V., Imbert, P., Viana, A., 1999. Seismic features diagnostic of contourite drifts. Marine Geology 162, 1-38.

Faugères, J., Stow, D.A.V., 1993a. Bottom-current-controlled sedimentation: A synthesis of the contourite problem. Sedimentary Geology 82.

Faugères, J.C., Stow, D.A.V., 1993b. Contourite drift types and their distribution in the North and South Atlantic Ocean basins. Sedimentary Geology 82, 189-203.

Faugères, J.C., Stow, D.A.V., 2008. Contourite drifts: Nature, Evolution and Controls, in: Rebesco, M., Camerlenghi, A. (Eds.), Contourites. Elsevier, pp. 259-288.

Flinch, J.F., 1993. Tectonic evolution of the Gibraltar Arc. Rice University, Houston, Texas, p. 381.

Foubert, A., Depreiter, D., Beck, T., Maignien, L., Pannemans, B., Frank, N., Blamart, D., Henriet, J.-P., 2008. Carbonate mounds in a mud volcano province off north-west Morocco: Key to processes and controls. Marine Geology 248, 74-96.

642

643 Frank, N., Ricard, E., Lutringer-Paquet, A., van der Land, C., Colin, C., Blamart, D., Foubert, A., Van
644 Rooij, D., Henriet, J.-P., de Haas, H., van Weering, T., 2009. The Holocene occurrence of cold water
645 corals in the NE Atlantic: Implications for coral carbonate mound evolution. Marine Geology 266,
646 129-142.

647

648 Frigola, J., Moreno, A., Cacho, I., Canals, M., Sierro, F.J., Flores, J.A., Grimalt, J.O., 2008. Evidence of
649 abrupt changes in Western Mediterranean Deep Water circulation during the last 50 kyr: A high-
650 resolution marine record from the Balearic Sea. Quaternary International 181, 88-104.

651

652 García, M., 2002. Caracterización morfológica del sistema de canales y valles submarinos del talud
653 medio del Golfo de Cádiz (SO de la Peninsula Iberica): Implecaciones oceanográficas., Facultad de
654 Ciencias de l Mar. Univ. Cádiz, Cádiz, p. 114.

655

656 García, M., Hernández-Molina, F.J., Llave, E., Stow, D.A.V., León, R., Fernández-Puga, M.C., Díaz del
657 Río, V., Somoza, L., 2009. Contourite erosive features caused by the Mediterranean Outflow Water in
658 the Gulf of Cadiz: Quaternary tectonic and oceanographic implications. Marine Geology 257, 24-40.

659

660 Gibbard, P.L., Head, M.J., Walker, M.J.C., 2010. Formal ratification of the Quaternary System/Period
661 and the Pleistocene Series/Epoch with a base at 2.58 Ma. Journal of Quaternary Science 25, 96-102.

662

663 Haffert, L., Haeckel, M., Liebetrau, V., Berndt, C., Hensen, C., Nuzzo, M., Reitz, A., Scholz, F.,
664 Schönfeld, J., Perez-Garcia, C., Weise, S.M., 2013. Fluid evolution and authigenic mineral paragenesis
665 related to salt diapirism – The Mercator mud volcano in the Gulf of Cadiz. Geochimica et
666 Cosmochimica Acta 106, 261-286.

667

668 Hans Nelson, C., Baraza, J., Maldonado, A., 1993. Mediterranean undercurrent sandy contourites,
669 Gulf of Cadiz, Spain. Sedimentary Geology 82, 103-131.
670
671 Haq, B.U., Hardenbol, J., Vail, P.R., 1987. Chronology of Fluctuating Sea Levels Since the Triassic.
672 Science 235, 1156-1167.
673
674 Heezen, B.C., Hollister, C.D., Ruddiman, W.F., 1966. Shaping of the continental rise by deep
675 geostrophic currents. Science 152, 502-508.
676
677 Hernández-Molina, F.J., Larter, R.D., Rebesco, M., Maldonado, A., 2006a. Miocene reversal of bottom
678 water flow along the Pacific Margin of the Antarctic Peninsula: Stratigraphic evidence from a
679 contourite sedimentary tail. Marine Geology 228, 93-116.
680
681 Hernández-Molina, F.J., Llave, E., Stow, D.A.V., García, M., Somoza, L., Vázquez, J.T., Lobo, F.J.,
682 Maestro, A., Díaz del Río, V., León, R., Medialdea, T., Gardner, J., 2006b. The contourite depositional
683 system of the Gulf of Cádiz: A sedimentary model related to the bottom current activity of the
684 Mediterranean outflow water and its interaction with the continental margin. Deep Sea Research
685 Part II: Topical Studies in Oceanography 53, 1420-1463.
686
687 Hernàndez-Molina, F.J., maldonado, A., Stow, D.A.V., 2008. Abyssal plain contourites, in: Rebesco,
688 M., Camerlenghi, A. (Eds.), Contourites. Elsevier, pp. 347-378.
689
690 Hernández-Molina, F.J., Serra, N., Stow, D.A.V., Llave, E., Ercilla, G., Van Rooij, D., 2011. Along-slope
691 oceanographic processes and sedimentary products around the Iberian margin. Geo-Mar Lett (in
692 press).
693

694 Hernández-Molina, F.J., Somoza, L., Vazquez, J.T., Lobo, F., Fernández-Puga, M.C., Llave, E., Díaz-del
695 Río, V., 2002. Quaternary stratigraphic stacking patterns on the continental shelves of the southern
696 Iberian Peninsula: their relationship with global climate and palaeoceanographic changes.
697 Quaternary International 92, 5-23.
698
699 Huvenne, V.A.I., De Mol, B., Henriet, J.P., 2003. A 3D seismic study of the morphology and spatial
700 distribution of buried coral banks in the Porcupine Basin, SW of Ireland. Marine Geology 198, 5-25.
701 Huybers, P., 2007. Glacial variability over the last two million years: an extended depth-derived
702 agemodel, continuous obliquity pacing, and the Pleistocene progression. Quaternary Science Reviews
703 26, 37-55.
704
705 Huybers, P., Wunsch, C., 2005. Obliquity pacing of the late Pleistocene glacial terminations. Nature
706 434, 491-494.
707
708 Iacono, C.L., Gràcia, E., Ranero, C.R., Emelianov, M., Huvenne, V., Bartolomé, R., Booth-Rea, G.,
709 Prades, J., the Melcor Cruise Party, accepted. The West Melilla Cold Water Coral Mounds, Eastern
710 Alboran Sea: Morphological characterization and environmental context. Deep Sea Research Part II:
711 Topical Studies in Oceanography.
712
713 Lisiecki, L.E., Raymo, M.E., 2005. A Plio-Pleistocene stack of 57 globally distributed benthic delta 18O
714 records. Paleoceanography 20, PA1003.
715
716 Llave, E., Hernández-Molina, F.J., Somoza, L., Díaz-del-Río, V., Stow, D.A.V., Maestro, A., Alveirinho
717 Dias, J.M., 2001. Seismic stacking pattern of the Faro-Albufeira contourite system (Gulf of Cadiz): a
718 Quaternary record of paleoceanographic and tectonic influences. Marine Geophysical Research 22,
719 487-508.

720

721 Llave, E., Hernández-Molina, F.J., Somoza, L., Stow, D.A.V., Díaz Del Río, V., 2007. Quaternary
722 evolution of the contourite depositional system in the Gulf of Cadiz. Geological Society, London,
723 Special Publications 276, 49-79.

724

725 Llave, E., Hernández-Molina, F.J., Stow, D.A.V., Somoza, L., Díaz-del-Río, V., 2005. The contourite
726 depositional system in the Gulf of Cadiz: an example of drifts with reservoir potential characteristics.
727 25 aniversario de la Asociación de Geólogos Geofisicos Españoles del Petróleo AAGGEP, Spec. Publ.,
728 53-73.

729

730 Llave, E., Matias, H., Hernández-Molina, F., Ercilla, G., Stow, D., Medialdea, T., 2011. Pliocene–
731 Quaternary contourites along the northern Gulf of Cadiz margin: sedimentary stacking pattern and
732 regional distribution. Geo-Marine Letters 31, 377-390.

733

734 Llave, E., Schönfeld, J., Hernández-Molina, F.J., Mulder, T., Somoza, L., Díaz del Río, V., Sánchez-
735 Almazo, I., 2006. High-resolution stratigraphy of the Mediterranean outflow contourite system in the
736 Gulf of Cadiz during the late Pleistocene: The impact of Heinrich events. Marine Geology 227, 241-
737 262.

738

739 Locker, S.D., Laine, E.P., 1992. Paleogene-Neogene depositional history of the middle U.S. Atlantic
740 continental rise: mixed turbidite and contourite depositional systems. Marine Geology 103, 137-164.

741

742 Louarn, E., Morin, P., 2011. Antarctic Intermediate Water influence on Mediterranean Sea Water
743 outflow. Deep Sea Research Part I: Oceanographic Research Papers 58, 932-942.

744

745 Lowrie, A., 1986. Model for fine-scale movements associated with climate and sea level changes
746 along the Louisiana shelfbreak growth faults. Gulf Coast Association Geological Societies Transactions
747 36, 497-508.
748
749 Maad, N., Le Roy, P., Sahabi, M., Gutscher, M.-A., Hssain, M., Babonneau, N., Rabineau, M., Lanoë,
750 B.V.V., 2010. Seismic stratigraphy of the NW Moroccan Atlantic continental shelf and Quaternary
751 deformation at the offshore termination of the southern Rif front. Comptes Rendus Geoscience 342,
752 731-740.
753
754 Machín, F., Hernández-Guerra, A., Pelegrí, J.L., 2006a. Mass fluxes in the Canary Basin. Progress In
755 Oceanography 70, 416-447.
756
757 Machín, F., Pelegrí, J.L., Marrero-Díaz, A., Laiz, I., Ratsimandresy, A.W., 2006b. Near-surface
758 circulation in the southern Gulf of Cádiz. Deep Sea Research Part II: Topical Studies in Oceanography
759 53, 1161-1181.
760
761 Maldonado, A., Somoza, L., Pallarés, L., 1999. The Betic orogen and the Iberian-African boundary in
762 the Gulf of Cadiz: geological evolution (central North Atlantic). Marine Geology 155, 9-43.
763
764 Marchès, E., Mulder, T., Gonthier, E., Cremer, M., Hanquiez, V., Garlan, T., Lecroart, P., 2010. Perched
765 lobe formation in the Gulf of Cadiz: Interactions between gravity processes and contour currents
766 (Algarve Margin, Southern Portugal). Sedimentary Geology 229, 81-94.
767
768 Mccave, I.N., Tucholke, B.E., 1986. Deep current-controlled sedimentation in the western North
769 Atlantic, in: McCreggor, B.A. (Ed.), The western North Atlantic region. The geological society of
770 America, pp. 451-468.

771

772 Medialdea, T., Somoza, L., Pinheiro, L.M., Fernández-Puga, M.C., Vázquez, J.T., León, R., Ivanov, M.K.,
773 Magalhaes, V., Díaz-del-Río, V., Vegas, R., 2009. Tectonics and mud volcano development in the Gulf
774 of Cádiz. Marine Geology 261, 48-63.

775

776 Medialdea, T., Vegas, R., Somoza, L., Vázquez, J.T., Maldonado, A., Día-del-Río, V., Maestro, A.,
777 Córdoba, D., Fernández-Puga, M.C., 2004. Structure and evolution of the "Olistostrome" complex of
778 the Gibraltar Arc in the Gulf of Cádiz (eastern Central Atlantic): evidence from two long seismic cross-
779 sections. Marine Geology 209, 173-198.

780

781 Mienis, F., De Stigter, H.C., De Haas, H., Van der Land, C., Van Weering, T.C.E., 2012. Hydrodynamic
782 conditions in a cold-water coral mound area on the Renard Ridge, southern Gulf of Cadiz. Journal of
783 Marine Systems 96–97, 61-71.

784

785 Millot, C., 2009. Another description of the Mediterranean Sea outflow. Progress In Oceanography
786 82, 101-124.

787

788 Perez-Garcia, C., Berndt, C., Klaeschen, D., Mienert, J., Haffert, L., Depreiter, D., Haeckel, M., 2011.
789 Linked halokinesis and mud volcanism at the Mercator mud volcano, Gulf of Cadiz. Journal of
790 Geophysical Research: Solid Earth 116, n/a-n/a.

791

792 Pinheiro, L.M., Ivanov, M.K., Sautkin, A., Akhmanov, G., Magalhães, V.H., Volkonskaya, A., Monteiro,
793 J.H., Somoza, L., Gardner, J., Hamouni, N., Cunha, M.R., 2003. Mud volcanism in the Gulf of Cadiz:
794 results from the TTR-10 cruise. Marine Geology 195, 131-151.

795

796 Pirlet, H., Wehrmann, L.M., Brunner, B., Frank, N., Dewanckele, J.A.N., Van Rooij, D., Foubert, A.,
797 Swennen, R., Naudts, L., Boone, M., Cnudde, V., Henriet, J.-P., 2010. Diagenetic formation of gypsum
798 and dolomite in a cold-water coral mound in the Porcupine Seabight, off Ireland. Sedimentology 57,
799 786-805.
800
801 Praeg, D., Ceramicola, S., Barbieri, R., Unnithan, V., Wardell, N., 2009. Tectonically-driven mud
802 volcanism since the late Pliocene on the Calabrian accretionary prism, central Mediterranean Sea.
803 Marine and Petroleum Geology 26, 1849-1865.
804
805 Preu, B., Hernández-Molina, F.J., Violante, R., Piola, A.R., Paterlini, C.M., Schwenk, T., Voigt, I.,
806 Krastel, S., Spiess, V., 2013. Morphosedimentary and hydrographic features of the northern
807 Argentine margin: The interplay between erosive, depositional and gravitational processes and its
808 conceptual implications. Deep Sea Research Part I: Oceanographic Research Papers 75, 157-174.
809
810 Rebesco, M., Hernández-Molina, F.J., van Rooij, D., Wåhlin, A., submitted. Contourites and associated
811 sediments controlled by deep-water circulation processes: State of the art and future considerations.
812 Marine Geology.
813
814 Rebesco, M., Richard, C.S., Cocks, L.R.M., Ian, R.P., 2005. Sedimentary environments: Contourites,
815 Encyclopedia of Geology. Elsevier, Oxford, pp. 513-528.
816
817 Richardson, P.L., Bower, A.S., Zenk, W., 2000. A census of Meddies tracked by floats. Progress In
818 Oceanography 45, 209-250.
819

820 Ridente, D., Trincardi, F., Piva, A., Asioli, A., 2009. The combined effect of sea level and supply during
821 Milankovitch cyclicity: Evidence from shallow-marine $\delta^{18}O$ records and sequence architecture
822 (Adriatic margin). Geology 37, 1003-1006.
823
824 Roque, C., Duarte, H., Terrinha, P., Valadares, V., Noiva, J., Cachão, M., Ferreira, J., Legoinha, P.,
825 Zitellini, N., 2012. Pliocene and Quaternary depositional model of the Algarve margin contourite
826 drifts (Gulf of Cadiz, SW Iberia): Seismic architecture, tectonic control and paleoceanographic
827 insights. Marine Geology 303–306, 42-62.
828
829 Schneider, E.D., Fox, P.J., Hollister, C.D., Needham, H.D., Heezen, B.C., 1967. Further evidence of
830 contour currents in the Western North Atlantic. Earth and Planetary Science Letters 2, 351-359.
831
832 Somoza, L., Díaz del Río, V., León, R., Ivanov, M., Fernández-Puga, M.C., Gardner, J.M., Hernández-
833 Molina, F.J., Pinheiro, L.M., Rodero, J., Lobato, A., Maestro, A., Vázquez, J.T., Medialdea, T.,
834 Fernández-Salas, L.M., 2003. Seabed morphology and hydrocarbon seepage in the Gulf of Cádiz mud
835 volcano area: Acoustic imagery, multibeam and ultra-high resolution seismic data. Marine Geology
836 195, 153-176.
837
838 Somoza, L., Medialdea, T., León, R., Ercilla, G., Vázquez, J.T., Farran, M.l., Hernández-Molina, J.,
839 González, J., Juan, C., Fernández-Puga, M.C., 2012. Structure of mud volcano systems and pockmarks
840 in the region of the Ceuta Contourite Depositional System (Western Alborán Sea). Marine Geology
841 332–334, 4-26.
842
843 Stow, D.A.V., Faugères, J.-C., Howe, J.A., Pudsey, C.J., Viana, A.R., 2002. Bottom currents, contourites
844 and deep-sea sediment drifts: current state-of-the-art. Geological Society, London, Memoirs 22, 7-20.
845

Stow, D.A.V., Hernández-Molina, F.J., 2006. Environmental significance of the Mediterranean outflow water and its global implications, IODP Full Proposal 644.

Stow, D.A.V., Hernández-Molina, F.J., Llave, E., Sayago, M., Díaz del Río, V., Branson, A., 2009. Bedform-velocity matrix: the estimation of bottom current velocity from bedform observations. Geology 37, 327-330.

Stow, D.A.V., Hunter, S., Wilkinson, D., Hernández-Molina, F.J., 2008. The nature of contourite deposition, in: Rebesco, M., Camerlenghi, A. (Eds.), Contourites. Elsevier.

Templer, S.P., Wehrmann, L.M., Zhang, Y., Vasconcelos, C., McKenzie, J.A., 2011. Microbial community composition and biogeochemical processes in cold-water coral carbonate mounds in the Gulf of Cadiz, on the Moroccan margin. Marine Geology 282, 138-148.

Tingay, M.R.P., Hillis, R.R., Morley, C.K., Swarbrick, R.E., Okpere, E.C., 2003. Pore pressure/stress coupling in Brunei Darussalam — implications for shale injection. Geological Society, London, Special Publications 216, 369-379.

Toucanne, S., Mulder, T., Schönfeld, J., Hanquiez, V., Gonthier, E., Duprat, J., Cremer, M., Zaragosi, S., 2007. Contourites of the Gulf of Cadiz: A high-resolution record of the paleocirculation of the Mediterranean outflow water during the last 50,000 years. Palaeogeography, Palaeoclimatology, Palaeoecology 246, 354-366.

Van Rensbergen, P., Depreiter, D., Pannemans, B., Moerkerke, G., Van Rooij, D., Marsset, B., Akhmanov, G., Blinova, V., Ivanov, M., Rachidi, M., Magalhaes, V., Pinheiro, L., Cunha, M., Henriet, J.-

P., 2005. The El Arraiche mud volcano field at the Moroccan Atlantic slope, Gulf of Cadiz. Marine Geology 219, 1-17.

Van Rooij, D., Blamart, D., De Mol, L., Mienis, F., Pirlet, H., Wehrmann, L.M., Barbieri, R., Maignien, L., Templer, S.P., de Haas, H., Hebbeln, D., Frank, N., Larmagnat, S., Stadnitskaia, A., Stivaletta, N., van Weering, T., Zhang, Y., Hamoumi, N., Cnudde, V., Duyck, P., Henriet, J.P., 2011. Cold-water coral mounds on the Pen Duick Escarpment, Gulf of Cadiz: The MiCROSYSTEMS project approach. Marine Geology 282, 102-117.

Van Rooij, D., Blamart, D., Richter, T., Wheeler, A., Kozachenko, M., Henriet, J.P., 2007. Quaternary sediment dynamics in the Belgica mound province, Porcupine Seabight: ice-rafting events and contour current processes. International Journal of Earth Sciences 96, 121-140.

Van Rooij, D., Iglesias, J., Hernández-Molina, F.J., Ercilla, G., Gomez-Ballesteros, M., Casas, D., Llave, E., De Hauwere, A., Garcia-Gil, S., Acosta, J., Henriet, J.P., 2010. The Le Danois Contourite Depositional System: Interactions between the Mediterranean Outflow Water and the upper Cantabrian slope (North Iberian margin). Marine Geology (2010) 274, 1-20.

van Weering, T.C.E., de Haas, H., de Stigter, H.C., Lykke-Andersen, H., Kouvaev, I., 2003. Structure and development of giant carbonate mounds at the SW and SE Rockall Trough margins, NE Atlantic Ocean. Marine Geology 198, 67-81.

Vandorpe, T., Van Rooij, D., Stow, D., Henriet, J.-P., 2011. Pliocene to Recent shallow-water contourite deposits on the shelf and shelf edge off south-western Mallorca, Spain. Geo-Marine Letters 31, 391-403.

Verdicchio, G., Trincardi, F., 2008. Shallow-water Contourites, in: Rebesco, M., Camerlenghi, A. (Eds.), Contourites. Elsevier, *Developments in Sedimentology*, pp. 409-433.

Viana, A.R., Almeida, W., Jr, Nunes, M.C.V., Bulhoes, E.M., 2007. The economic importance of contourites. Geological Society, London, Special Publications 276, 1-23.

Viana, A.R., Faugeres, J.C., Kowsmann, R.O., Lima, J.A.M., Caddah, L.F.G., Rizzo, J.G., 1998a. Hydrology, morphology and sedimentology of the Campos continental margin, offshore Brazil. Sedimentary Geology 115, 133-157.

Viana, A.R., Faugères, J.C., Stow, D.A.V., 1998b. Bottom-current-controlled sand deposits -- a review of modern shallow- to deep-water environments. Sedimentary Geology 115, 53-80.

Wehrmann, L.M., Templer, S.P., Brunner, B., Bernasconi, S.M., Maignien, L., Ferdelman, T.G., 2011. The imprint of methane seepage on the geochemical record and early diagenetic processes in cold-water coral mounds on Pen Duick Escarpment, Gulf of Cadiz. Marine Geology 282, 118-137.

Wienberg, C., Frank, N., Mertens, K.N., Stuut, J.-B., Marchant, M., Fietzke, J., Mienis, F., Hebbeln, D., 2010. Glacial cold-water coral growth in the Gulf of Cádiz: Implications of increased palaeo-productivity. Earth and Planetary Science Letters 298, 405-416.

Wienberg, C., Hebbeln, D., Fink, H.G., Mienis, F., Dorschel, B., Vertino, A., Correa, M.L., Freiwald, A., 2009. Scleractinian cold-water corals in the Gulf of Cádiz—First clues about their spatial and temporal distribution. Deep Sea Research Part I: Oceanographic Research Papers 56, 1873-1893.

Figure Captions

Fig. 1: Overview of the oceanic circulation and main geological features within the Gulf of Cadiz. The white dots represent mud volcanoes within the Spanish-Portuguese mud volcano field (SPM) and the white circle with a dot is the Lolita salt diapir. The transparent white box indicates the investigated area (Fig. 2) and the double arrow shows the transect of the CTD profile (Fig. 3). a: Donana diapiric ridge, b: Cadiz diapiric ridge, GDR: Guadalquivir mud volcano field, DPM: Deep Portuguese mud volcano field, UC: MOW upper current, IB: MOW intermediate branch, PB: MOW principal branch, SB: MOW southern branch, MOW: Mediterranean Outflow Water, AAIW: Antarctic Intermediate Water, NACW: North Atlantic Central Water, NADW: North Atlantic Deep Water

Fig. 2: Topographic features in the Pen Duick area and location of the discussed seismic profiles. The inset shows the topography perpendicular to the Gemini mud volcano. The black arrows indicate the position of the moats and the inferred direction of the current within them. The white dots indicate the six mounds at the base of the PDE, while the white circles indicate alpha (most southern), beta (central) and gamma (most northern) mound. LdT: Lazarillo del Torres (mud volcano). Multibeam bathymetry discussed by Van Rensbergen et al. (2005).

Fig. 3: A) Salinity (colors) and temperature (contours, °C) transect 10-15 km south of the Gemini Mud Volcano and Pen Duick Escarpment (PDE). The data were obtained from the world ocean database (World Ocean Database, 05/02/2013). B) Salinity-temperature plot of used CTD stations. NASW is characterized by high temperature an salinity values, NACW by a decreasing line on the T-S plot and decreasing temperatures and salinities in the transect. AAIW lies on a line of increasing salinities In the transect, is is characterized by slightly higher salinity values compared to the NACW. The MOW is characterized by high salinity values (Louarn and Morin, 2011; Machín et al., 2006b).

Fig. 4: Multichannel airgun seismic profile (and interpretation) displaying 5 seismic stratigraphic units. Unit 1 and the upper part of Unit 2 have been interpreted, the upper units are displayed in a greater detail in Figs. 5, 6 and 7. A large fault is present in the centre of the profile and smaller ones to the southwest. The lower part of the large fault is concealed by the chaotic expression of the deposits. The small arrow in the ENE indicates the infill progradation of the depression (within the black box).

Fig. 5: Single channel sparker seismic profile (and interpretation) perpendicular to the Gemini mud volcano, displaying 4 out of 5 units. The lower boundary of Unit 2 is based on correlation with other profiles. Relative current strengths are indicated by the size of the bottom current symbol and the green arrow shows the increase in mounded nature of the deposits of Unit 3. The green fillings in the NNE indicate when mud eruptions did not occur and sediments are deposited on top of the mud. The table at the left side of the figure consists of the unit, subunit and the marine isotopic stage (MIS) in which the unit is deposited.

Fig. 6: Single channel sparker seismic profile (and interpretation) perpendicular to the Pen Duick escarpment (PDE), displaying 4 out of 5 units. The green arrow indicates the increase in mounded nature of the sediments in Unit 3. The same table as for Fig. 5 is used. Relative currents strengths are indicated by the size of the symbol.

Fig. 7: Single channel sparker seismic profile (and interpretation) perpendicular to the Pen Duick escarpment, across one of the mounds at its foot (Fig. 2). The green spots within Unit 3 indicate buried cold-water coral mounds (CWC) and the green dotted part in the mound on top of the sediment indicates the CWC part of that mound. The yellow part of Unit 5 shows the mounded sediment drift WSW of the mound. A bottom current flows along PDE and mound.

Fig. 8: Isopach maps of Units 2 to 5. The thicknesses are displayed in ms TWT (two-way travel time). On each map, the Pen Duick escarpment and Gemini mud volcano are indicated. The uplift of the PDE can be seen by the reduced thickness at its foot.

Fig. 9: Summarizing sketches of the contourite drift evolution along both Pen Duick escarpment (right panels) and Gemini mud volcano (left panels). Relative bottom current strengths are indicated by the size of the symbol. The dark orange part indicate active mud flows from the Gemini MW. The sketch within Unit 5 along the PDE shows the build-up of the mounds at the foot of the PDE.

Fig. 10: Comparison of the evolution of the Pen Duick drift to MOW-controlled drifts in the northern Gulf of Cadiz (Roque et al., 2012) and the Bay of Biscay (Van Rooij et al., 2010). Red boxes stand for pre-contourite deposits, yellow for sheeted drift and green for mounded drift deposits. MIS: Marine Isotopic Stage.

Figure 1

Click here to download high resolution image

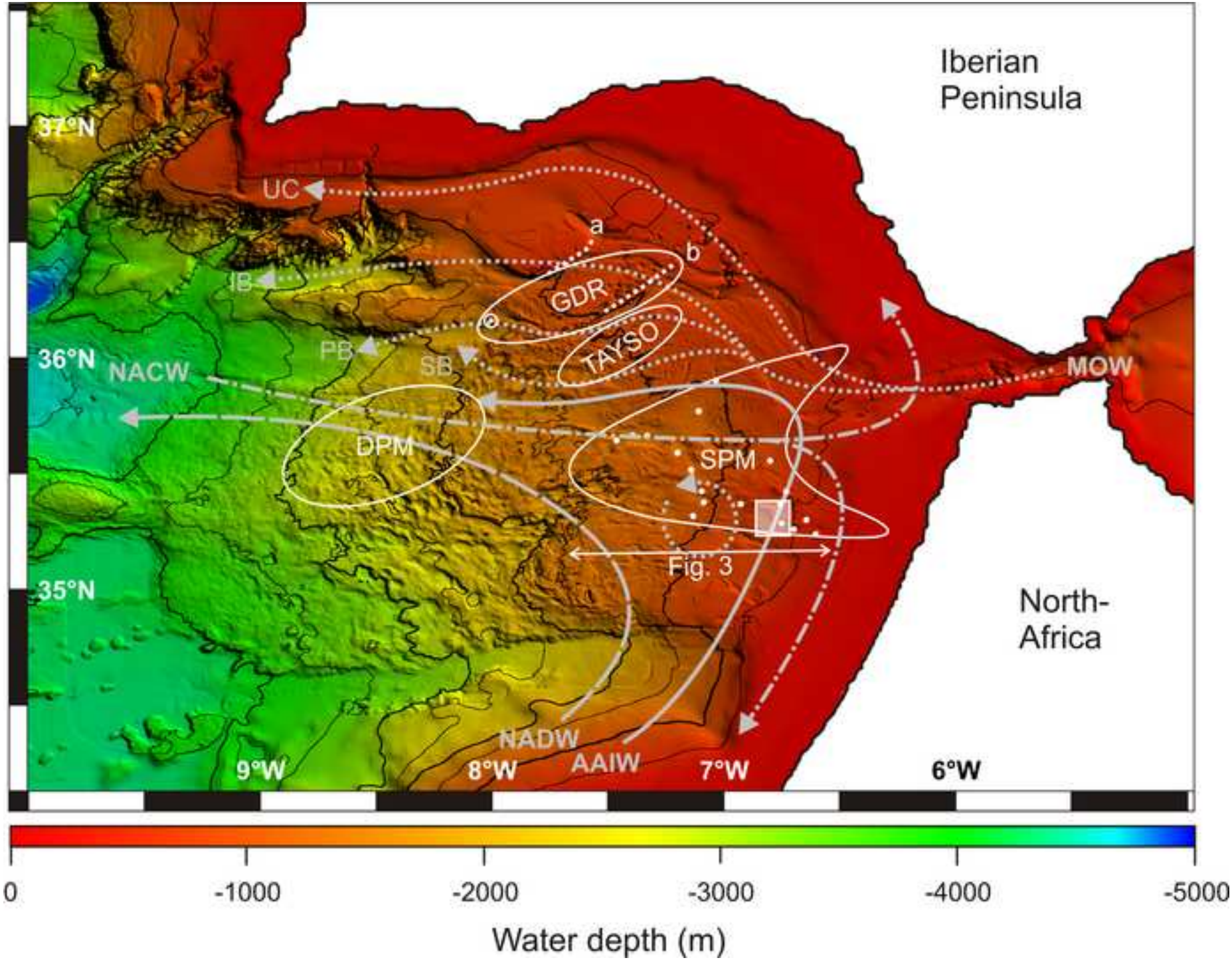

Figure 2

Click here to download high resolution image

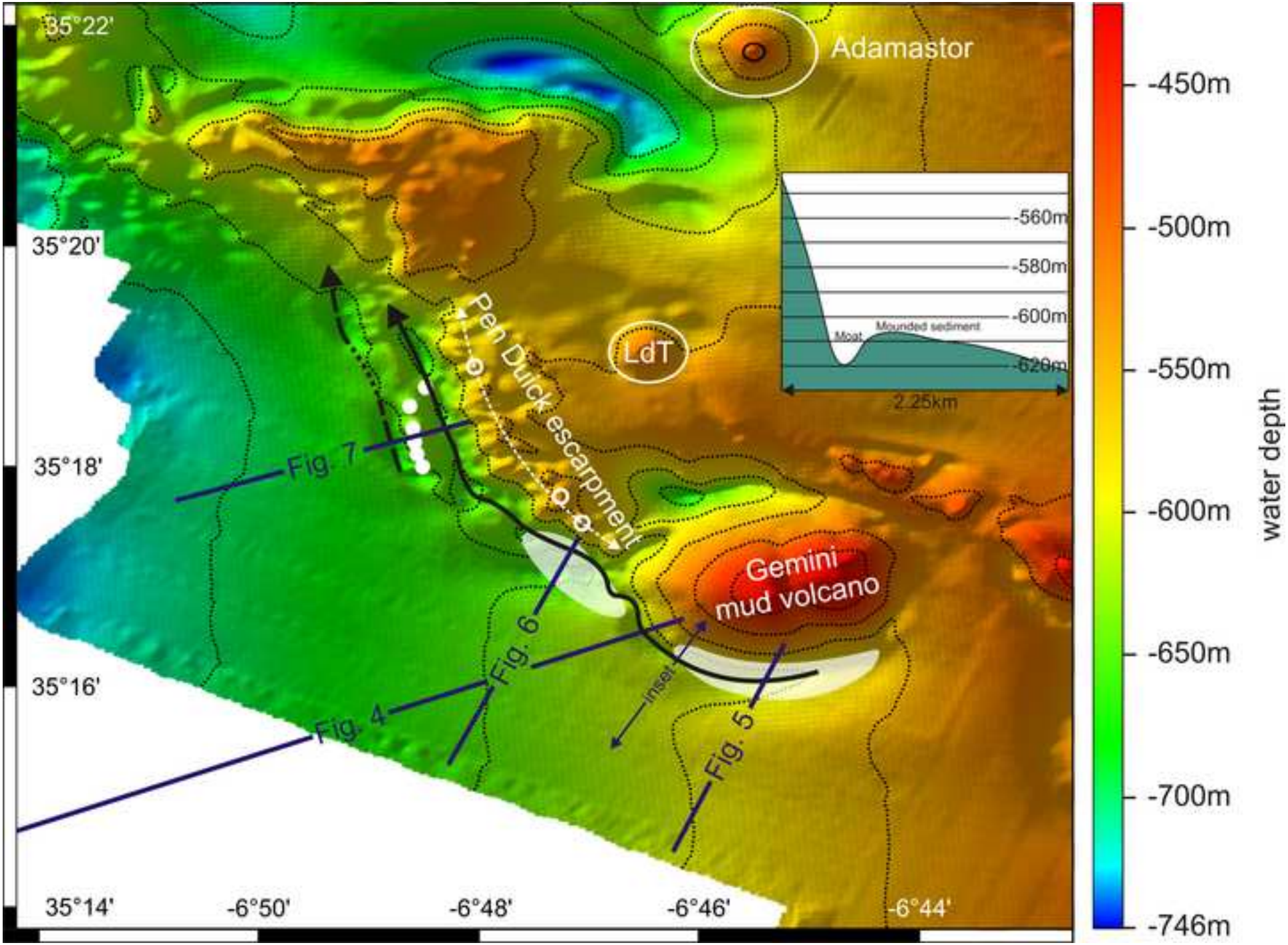

Figure 3

Click here to download high resolution image

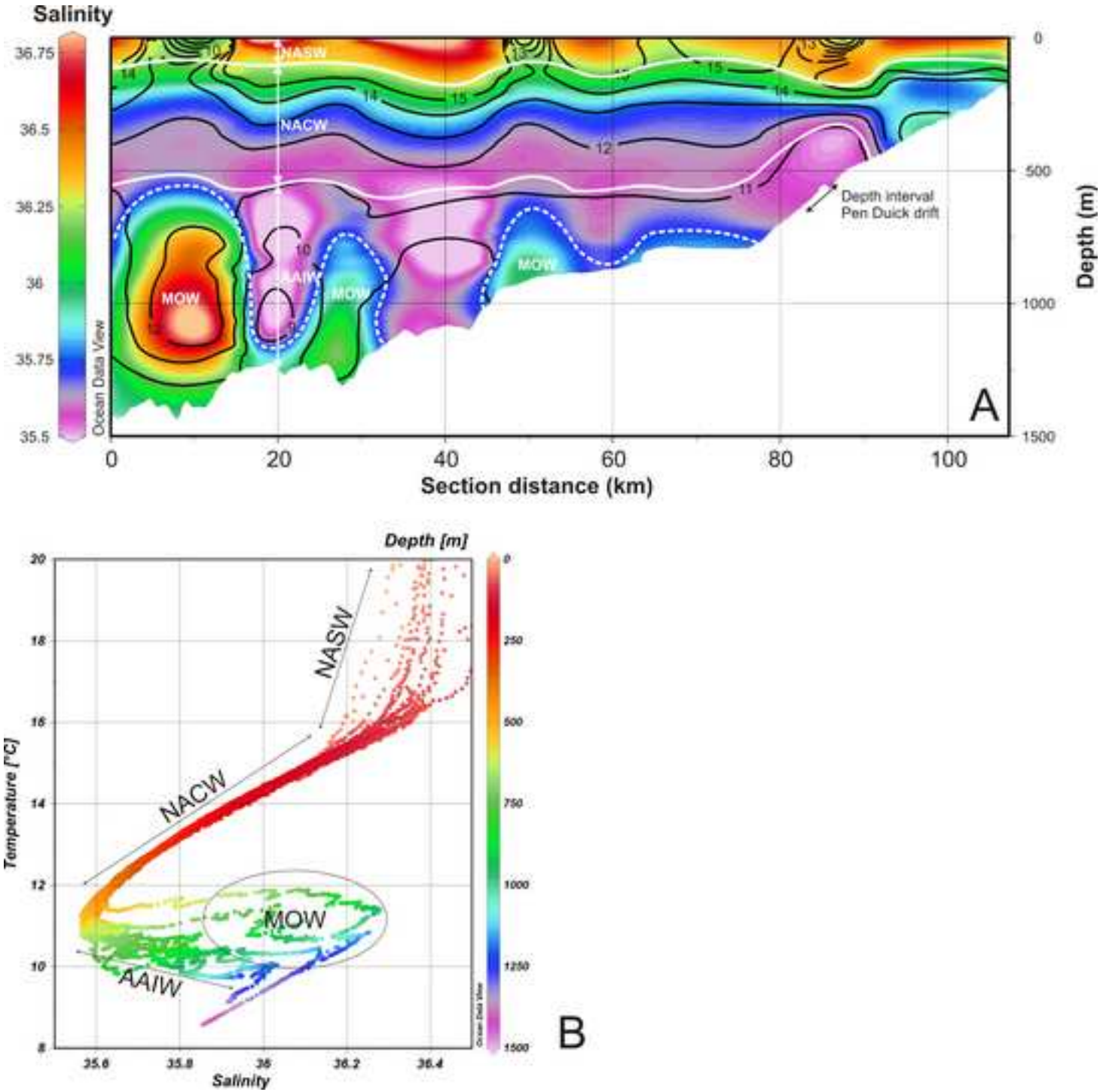

Figure 4

Click here to download high resolution image

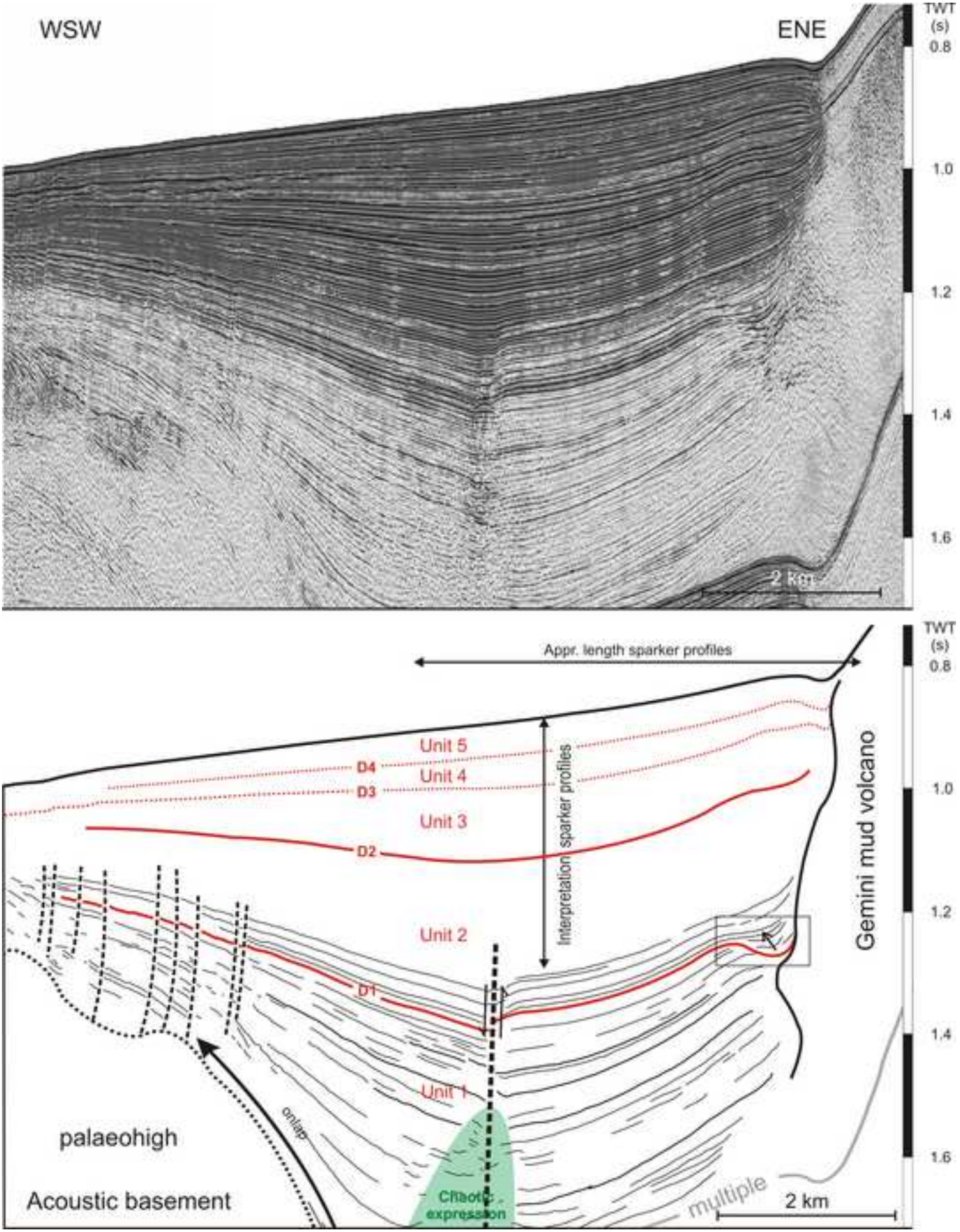

Figure 5

Click here to download high resolution image

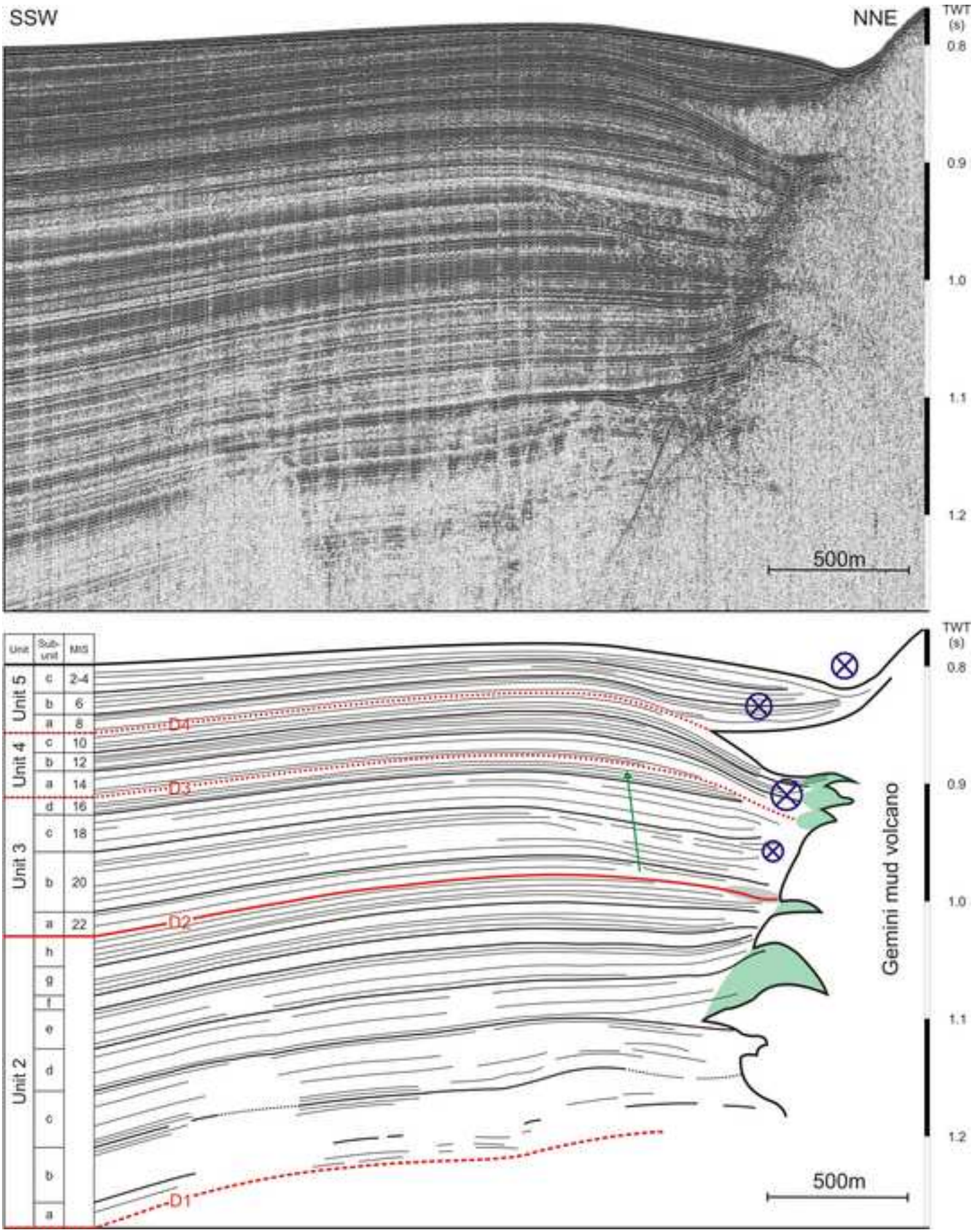

Figure 6

Click here to download high resolution image

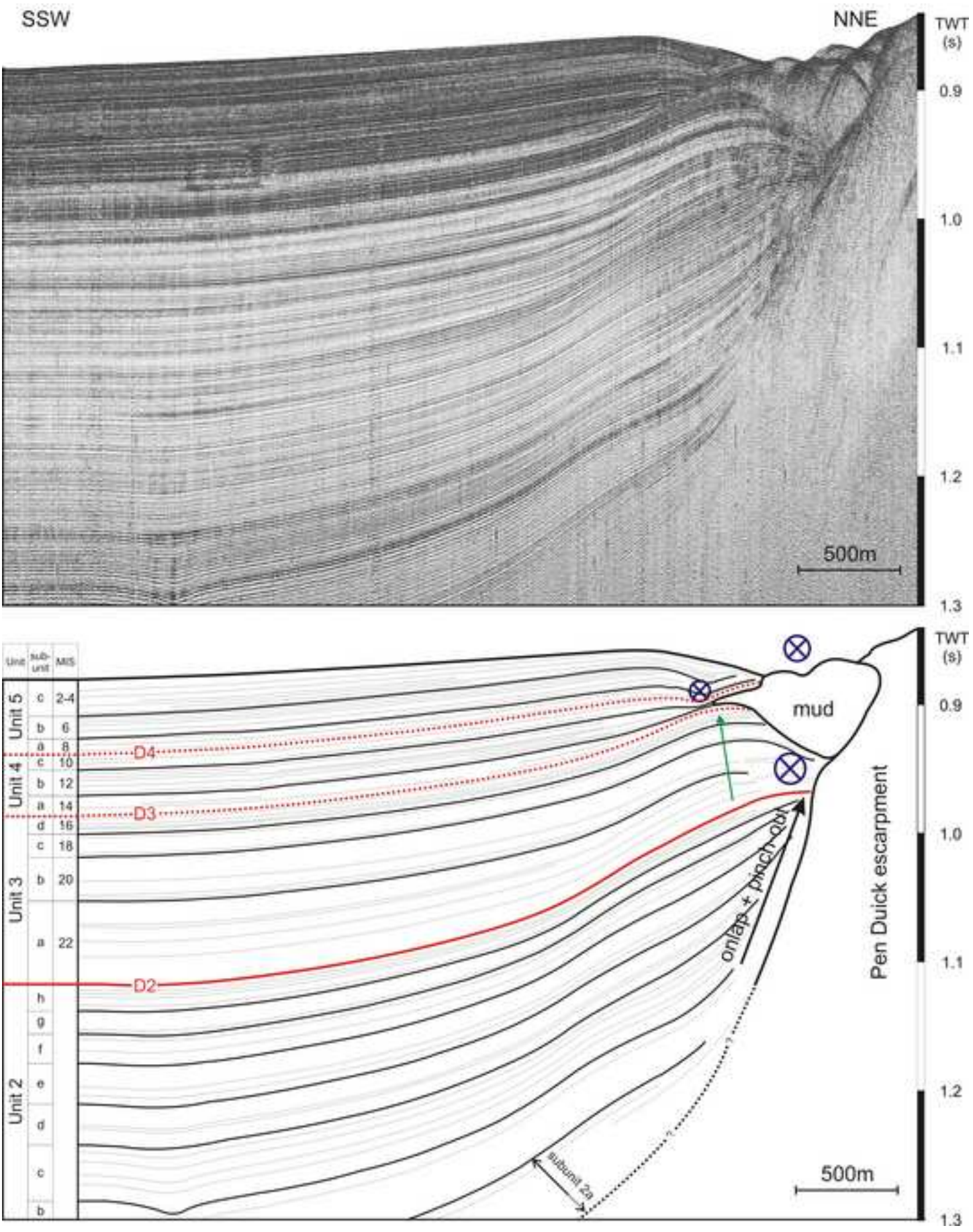

Figure 7

Click here to download high resolution image

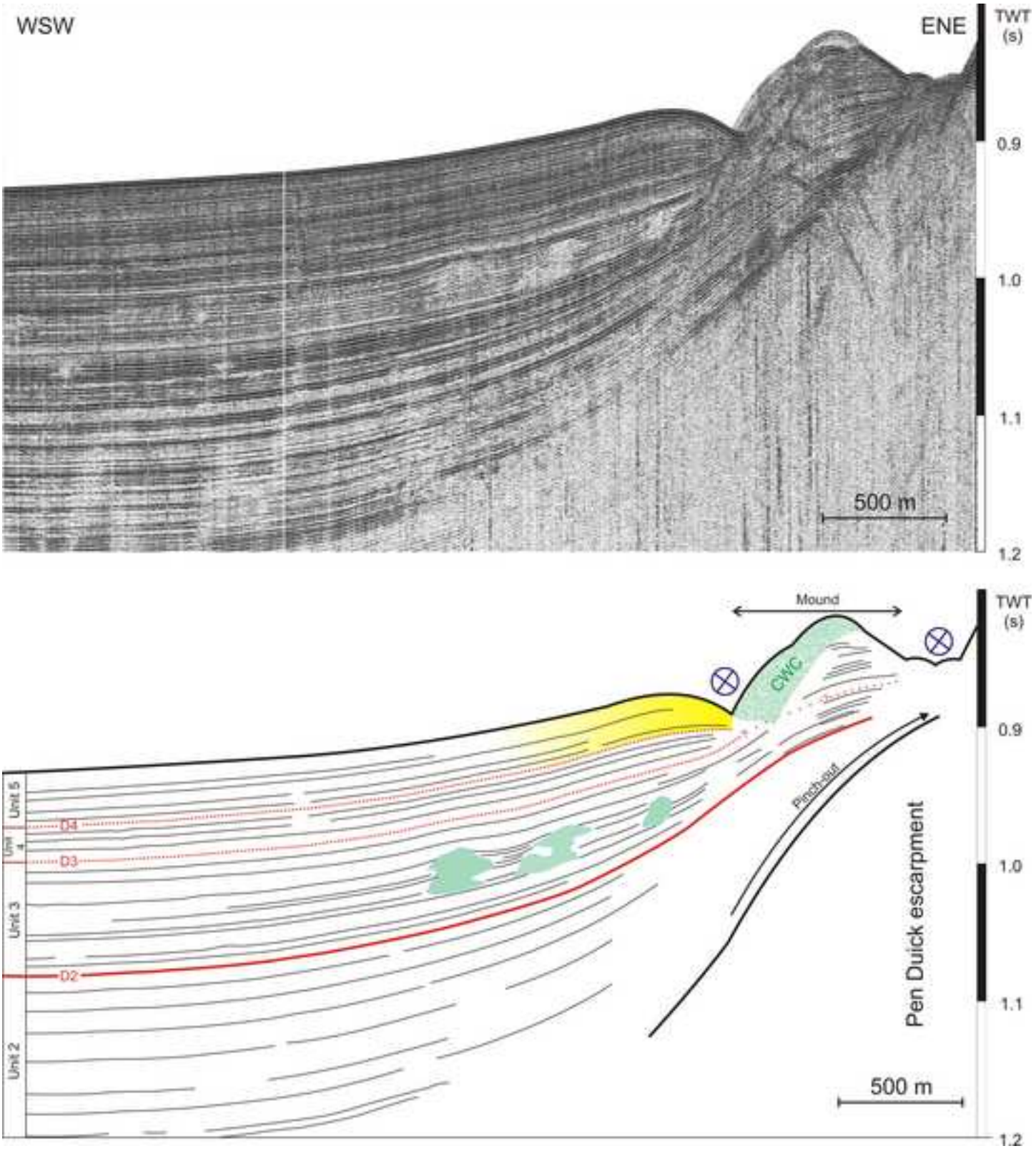

Figure 8

Click here to download high resolution image

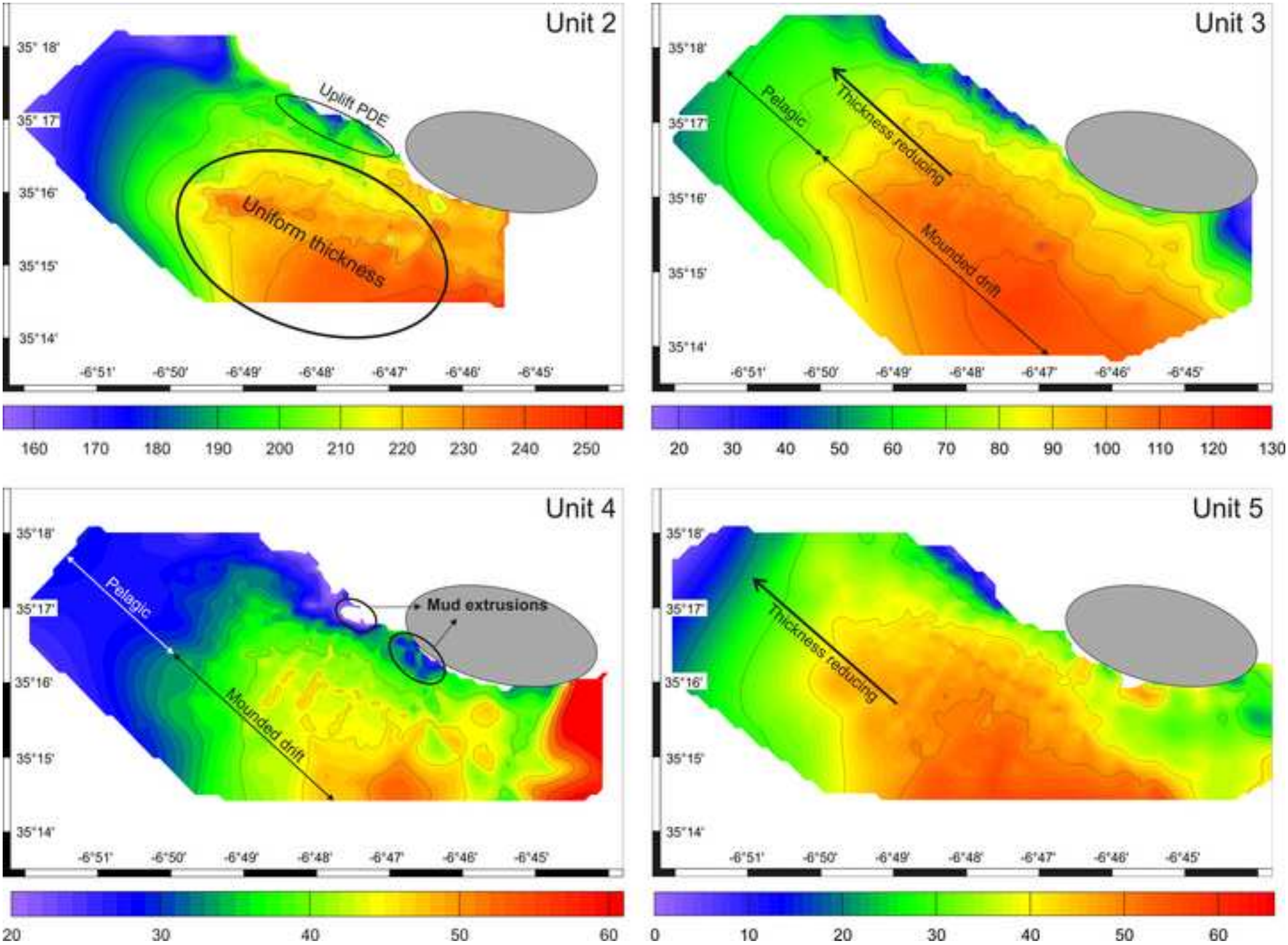

Figure 9

Click here to download high resolution image

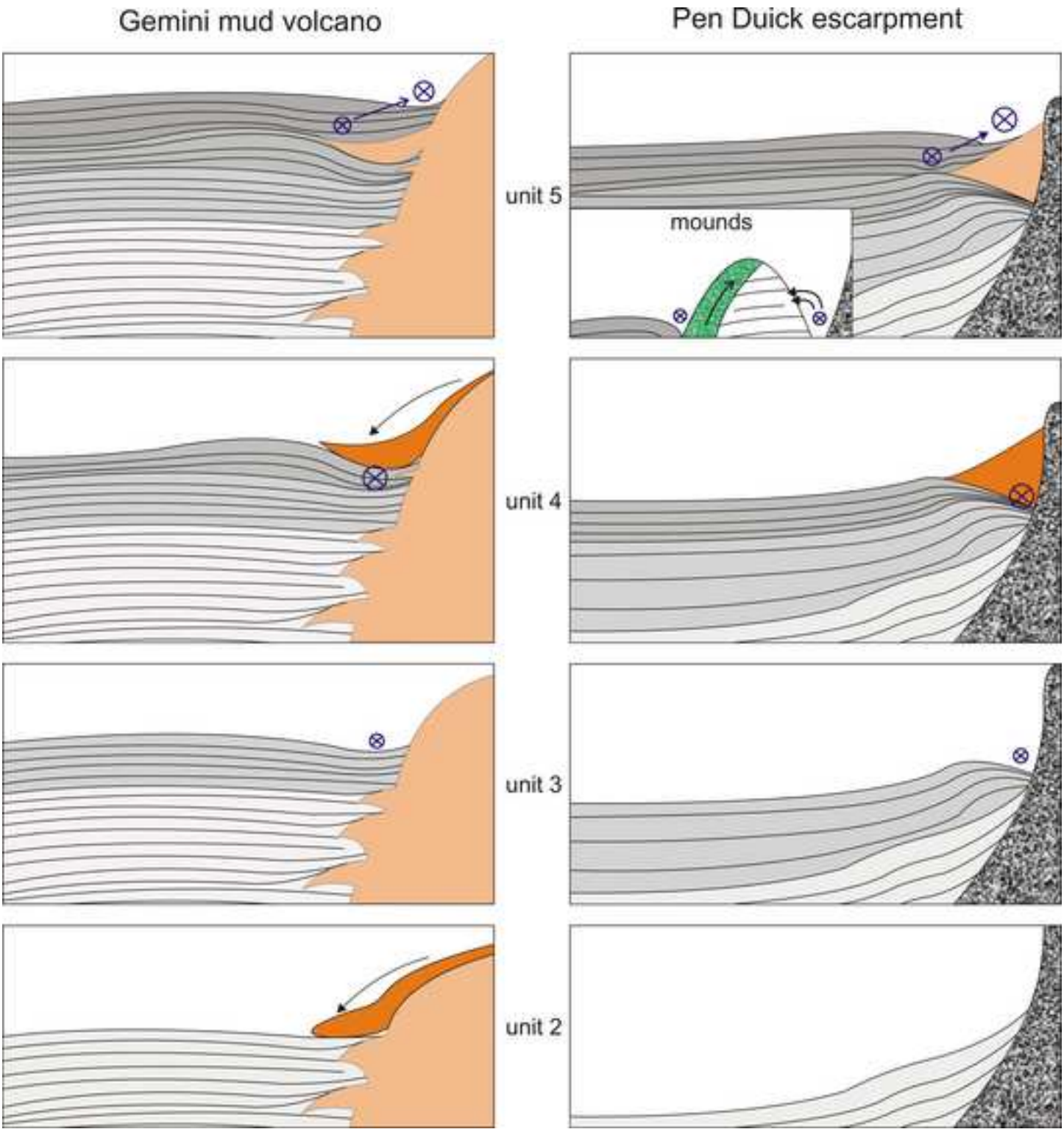

Figure 10

Click here to download high resolution image